Title

High-Pressure Thermal Isotropic Cell for Evaluation of Thermal Volume Change of Soils

Journal

Geotechnical Testing Journal, 39(2)

ISSN

0149-6115

Authors

Coccia, Charles James Russell
McCartney, John S

Publication Date

2016-03-01

DOI

10.1520/gtj20150114

Peer reviewed

High-Pressure Thermal Isotropic Cell for Evaluation of Thermal Volume Change of Soils

Charles James Russell Coccia, M.S., Doctoral Candidate
University of Colorado Boulder, Dept. of Civil, Environmental and Architectural Engineering
UCB 428, Boulder, CO 80309; coccia@colorado.edu
John S. McCartney, Ph.D., P.E., Associate Professor
University of California San Diego, Dept. of Structural Engineering
9500 Gilman Dr., La Jolla, CA 92093-0085; mccartney@ucsd.edu

ABSTRACT: This paper describes a new high pressure, temperature-controlled isotropic cell used for evaluation of the thermal volume change mechanisms of saturated and unsaturated soils under isotropic stress states. Specifically, details of the experimental setup, instrumentation, thermo-mechanical calibration of the device, experimental procedures, and typical results are presented in this paper. The thermal isotropic cell includes suction control using the axis translation technique, saturation control/monitoring using a pore water pressure flow pump, cell pressure control using a high pressure flow pump, and a stainless steel cell to permit application of isotropic net mean stresses up to 10 MPa. The cell fluid temperature is regulated by circulating heated water through a copper heating coil within the cell, and an internal circulating fan is used to promote homogenous temperature throughout the cell chamber. Non-contact proximity transducers are used to directly measure soil deformation in the radial and axial directions, permitting assessment of thermo-mechanical anisotropic strains during changes in mean effective stress or temperature while also avoiding the need to consider complex thermo-mechanical cell deformations. The high pressure flow pump and thermal control system are designed to apply changes in net mean stress and temperature at slow rates in order to characterize the full soil compression and thermal volume change curves, respectively. Along with the thermo-mechanical calibration of the cell, the results from two tests on compacted silt specimen having different initial degrees of saturation are presented that show how the cell can be used to characterize changes in volume and degree of saturation during thermo-mechanical loading. Both normally consolidated soil specimens were contracted during heating, although the specimen with a lower degree of saturation showed slightly greater thermal volume change.

KEYWORDS: Thermal isotropic cell, thermo-mechanical testing, non-isothermal, volume change

INTRODUCTION

The thermal volume change behavior of saturated and unsaturated soils is gaining interest due to the incorporation of ground source heat exchangers into geotechnical engineering infrastructure. Examples of such applications involving soils exposed to elevated temperatures include energy piles (Murphy et al. 2015), thermally active soil embankments (Coccia and McCartney 2013), and thermally active mechanically stabilized earth (MSE) walls (Stewart et al. 2014). Several studies have evaluated the thermo-mechanical behavior of saturated soil (Campanella and Mitchell 1968; Demars and Charles 1982; Hueckel and Baldi 1990; Towhata et al. 1993; Burghignoli et al. 2000; Sultan et al. 2002; Cekerevac and Laloui 2004) and unsaturated soils (Romero 1999; Romero et al. 2005; Salager et al. 2008; Tang et al. 2008; Uchaipichat and Khalili 2009). In these studies, the thermal volume change behavior of unsaturated soil is typically investigated in light of the applied net stress and matric suction. Further, very few studies have investigated the impact of the degree of saturation on the thermal response of unsaturated soils as well as the evolution of the degree of saturation during heating under constant suction conditions (Romero 1999). Recently, the degree of saturation has been used as a key parameter in predicting the mechanical behavior of unsaturated soils and may be more useful in characterizing changes in unsaturated soil behavior than matric suction (Wheeler et al. 2003; Zhou et al. 2012; Bellia et al. 2015). As such, the degree of saturation may also influence the thermal volume change response, as well as the resulting mechanical response following heating. A deeper understanding of this topic will aid in the development and calibration of thermo-elasto-plastic constitutive models for soils under non-isothermal conditions, especially for those which utilize degree of saturation as a state variable.

Although testing equipment and procedures have been developed to characterize the thermal volume change of saturated soils (Campanella and Mitchell 1968, Demars and Charles 1982,

Sultan et al. 2002, Cekerevac and Laloui 2004; Coccia and McCartney 2012; Vega and McCartney 2014) and unsaturated soils (Romero 1999; Romero et al. 2001; Salager et al. 2008; Tang 2005; Tang et al. 2008; Uchaipichat et al. 2011; Alsherif and McCartney 2015), challenges still remain in the measurement of thermal volume change under various stress states and the associated changes in thermo-mechanical behavior, as well as the evolution and resulting influence of degree of saturation. Furthermore, most current volume measurement techniques require large and complex thermo-mechanical calibrations and do not have the ability to directly measure strain anisotropy of the soil during changes in mean effective stress or temperature (Huckel and Pellegrini 1996; Coccia and McCartney 2012). The objective of this paper is to present a new high pressure thermal isotropic cell capable of measuring the thermal volume change behavior of saturated and unsaturated soils under different stress histories while simultaneously monitoring changes in degree of saturation and developments of strain anisotropy. To showcase the capabilities of the new thermal testing equipment, the thermo-mechanical machine deformations of the thermal isotropic cell along with some typical results from heating tests performed on specimens of compacted silt having different initial degrees of saturation are presented.

BACKGROUND

Several studies have been performed to define the impact of temperature on the volume change behavior of saturated soils (Paaswell 1967; Plum and Esrig 1969; Demars and Charles 1982; Baldi et al. 1988; Hueckel and Baldi 1990; Hueckel and Pellegrini 1992; Towhata et al. 1993; Delage et al. 2000; Cekerevac and Laloui 2004). The overall goal of these studies was to identify the recoverable (elastic) and irrecoverable (plastic) deformations of different types of soils during heating and cooling. Stress history, characterized by the overconsolidation ratio

(OCR), is observed to play an important role in the thermal volume change behavior of soils. For poorly draining (i.e. low hydraulic conductivity), normally consolidated (OCR = 1) and lightly overconsolidated saturated soils heated under drained conditions, differential expansion of pore water and soil particles may lead to a generation of excess pore water pressure if the thermal expansion of the pore water occurs at a rate faster than it is able to drain from the soil pore network. This will result in a temporary expansion of the soil volume, followed by irrecoverable volumetric contraction as the thermally induced excess pore water dissipates with time as a function of the soil's hydraulic conductivity (Delage et al. 2000). This response is similar to primary consolidation during application of a change in total stress (Campanella and Mitchell 1968; Cui et al. 2000; Delage et al. 2000; Cui et al. 2009). Likewise, for normally consolidated soils heated at slow heating rates, irreversible volumetric contraction will occur due to a decrease in inter-particle shearing strength due to the increase in temperature as explained by Campanella and Mitchell (1968). This decrease in inter-particle shearing strength (or bond strength) may be considered as a result from the increase in thermal energy due to heating, resulting in a collapse of the soil skeleton, ultimately reducing the void ratio of the specimen. This is analogous to secondary compression behavior observed after mechanical primary consolidation and will continue until enough new bonds are developed which can carry the thermo-mechanically induced stresses. For soils with larger OCRs, reversible thermal expansion is typically observed, followed by irreversible thermal contraction (Cekerevac and Laloui 2004). The OCR has also been observed to play a similar role in unsaturated soils (Romero 1999; Saix et al. 2000; Romero et al. 2005; Tang 2005; Tavallali et al. 2007; François and Laloui 2008; Tang et al. 2008; Uchaipichat and Khalili 2009). In isotropic stress conditions, strain anisotropy, defined as the ratio of axial strain to radial strain, may develop during heating (Baldi et al. 1991; Del-Olmo et

al. 1996; and Hueckel and Pellegrini 1996). Del-Olmo et al. (1996) assessed the strain anisotropy of deep Spanish clay during drained heating under isotropic conditions. In this study, thermal axial strains (ε_{aT}) were deduced directly by axial piston displacements while thermal radial strains (ε_{rT}) were determined indirectly based on the measured thermal volumetric (ε_{vT}) and thermal axial strains using the relationship as defined in Eq. 1:

$$\varepsilon_{rT} = \frac{1}{2\left(\varepsilon_{vT} - \varepsilon_{aT}\right)} \qquad \text{EQ. 1}$$

During heating and cooling, Del-Olmo et al. (1996) observed thermally induced strains to be larger in the radial direction than in the axial direction. Similar findings were also observed by Baldi et al. (1991). Generally, thermal strain anisotropy may be attributed to the inherent structural anisotropy of the soil specimen due to compaction (Hueckel and Pellegrini 1996). However, Baldi et al. (1991) observed strains in the radial direction to still dominate the overall thermal volume change response for undisturbed specimens of Boom clay that had been trimmed in the horizontal direction to directly measure thermal strains in the soil's natural horizontal direction. Interestingly, the values of strain in the radial and axial directions are nearly equal for the vertically and horizontally trimmed Boom clay specimens. Similarity among the two tests by Baldi et al. (1991) may be attributed to one of two explanations: (1) The structural arrangement of the soil skeleton does not directly impact the magnitude of thermal strains in the axial or radial directions, or; (2) The influence of the orientation of the soil skeleton has been dominated by the thermal equipment calibrations utilized to deduce changes in soil volume or height. However, it is difficult to draw a definite conclusion regarding thermal strain anisotropy without performing tests utilizing an experimental device capable of directly measuring both thermal axial and radial strain (Hueckel and Pellegrini 1996).

A few studies have also focused on the impact of changes in temperature and matric suction on preconsolidation stress (Tidfors and Sällfors 1989; Salager et al. 2008; Uchaipichat and Khalili 2009). Salager et al. (2008). These studies generally observed that increases in temperature cause a decrease in the mean preconsolidation stress while increases in matric suction beyond the air entry value resulted in an increase in the mean preconsolidation stress. This behavior was also observed for unsaturated soils by Uchaipichat and Khalili (2009).

To analyze the thermal volume change behavior of soils, several devices have been developed by incorporating temperature control equipment into oedometers (Paaswell 1967; Plum and Esrig 1969; Towhata et al. 1993; Romero 1999; Salager et al. 2008), isotropic cells (Tang et al. 2006; Salager et al. 2008), or triaxial cells (Campanella and Mitchell 1968; Demars and Charles 1982; Sultan et al. 2002; Cekerevac et al. 2005; Uchaipichat and Khalili 2009). For saturated soils, volume change measurements can be made by monitoring changes in the soil height in the case of modified thermal oedometers (Plum and Esrig 1969), or by measuring changes in pore water volume in the use of thermal isotropic cells or triaxial cells (Cekerevac et al. 2005). For unsaturated soils, thermal volume change measurement becomes more difficult due to the inclusion of air into the soil pore network. In such case, measurement of the specimen volume change may no longer be accomplished through measurement of the changes in pore water itself, changes in volume of the pore air must also be accounted for. However, due to the high compressibility air, its sensitivity to temperature, and the potential for air to diffuse through the membrane surrounding the soil specimen, this can yield very unreliable results. To overcome this limitation, several techniques have been developed to measure the thermal volume change of unsaturated soils including the cell fluid volume measurement technique (Tang et al. 2008; Alsherif and McCartney 2013), the digital imaging technique (Uchaipichat et al. 2011), and the

direct measurement technique using contact or non-contact displacement transducers (Salager et al. 2008).

For the cell fluid volume measurement technique, changes in volume of the soil specimen are inferred from movement of the cell fluid into or out of the cell (Bishop and Donald 1961). Movement of the cell fluid may be tracked using a flow pump device or high accuracy burette measuring system. A drawback of this method is that the overall volume change of cell fluid due to changes in soil volume will encounter additional fluctuations due to the accompanying changes in volume of the experimental equipment including: the cylindrical cell chamber, coarse stones, HAEV disks, plumbing lines (air, water, and cell pressure), water exposed to variable temperature during testing, and volume change measurement equipment itself (i.e. flow pump reservoir, burette shell, internal fluid). In addition, room temperature fluctuations will grossly affect the cell fluid volume measured using either a flow pump device or burette due to the thermal expansion of the fluid located between the chamber cell and the measuring device. These additional volume fluctuations may lead to unreliable results if not properly accounted for, thereby requiring an intensive calibration program.

The digital imaging technique utilizes a high-resolution photo or video camera to track the exterior profile of the soil specimen subjected to various stress paths. Images may be taken at a specified time increment dependent on the speed of loading chosen. Each image captured is then broken down into unique pixels that are each assigned a numerical location. Movement of each pixel is tracked using computer software (Macari et al. 1997) and changes in the overall profile may be associated to a change in soil volume. A drawback of this approach is the necessity for a transparent cell wall so that imaging of the soil specimen may take place. This necessity can limit the maximum confining pressure capabilities of the cell due to the need for a transparent

material. Likewise, thermal insulation and interior experimental equipment may not obstruct view of the specimen, as it would additionally hinder the ability to capture clean images of the soil specimen. Further discussion of the digital imaging technique may be found in Uchaipichat et al. (2011).

Salager et al. (2008) employed the direct measurement technique using two non-contact displacement sensors to track changes in soil height and diameter. The proximity sensors use induction to infer the distance between an aluminum target and a coil embedded within the tip of the proximity probe. A change in gap between the probe tip and target produces a perturbation in the magnetic field of the coil, resulting in a change in the output voltage. However, due to the probes' use of inductance to determine changes in distance between the probe tip and target, water cannot be used as the cell fluid as it will cause interference amongst the operating probes within the cell. As such, Salager et al. (2008) utilized air as the confining cell fluid and temperature was controlled using electrical resistances installed into the isotropic cell frame. A drawback of this approach, however, is a much larger time is required to heat the specimen due to the much lower thermal conductivity of air compared to that of de-aired water or oil.

HIGH PRESSURE THERMAL ISOTROPIC CELL

Overview

A new isotropic cell was designed to control and measure elevated temperatures and low suction magnitudes (0 to 100 kPa) for a broad range of OCRs. In the development of this new experimental system, efforts were made to improve the volume change measurement capabilities over existing thermal systems. Specifically, these improvements include the ability to directly measure changes in soil volume during heating while avoiding the reliance on large and sensitive thermo-mechanical calibrations via use of non-contact displacement transducers. Mineral oil has

been selected for the cell fluid to enhance the temperature application abilities of the system when compared to the system of Salager et al. (2008) who also used non-contact displacement transducers with air as the cell fluid. Another capability of this volume change measurement approach is the direct measurement of both axial and radial strains to assess strain anisotropy due to changes in mean effective stress or temperature which may be used to clarify the thermal anisotropic strain behaviors discussed by Hueckel and Pellegrini (1996). Additional benefits of the new thermal system include the ability to reliably monitor and control the degree of saturation due to changes in temperature as well as apply slow heating and mechanical loading rates to avoid the generation of excess pore water pressures for poorly draining soils.

To examine the thermal volume change mechanisms of saturated and unsaturated soils, the testing equipment must be capable of independently controlling and monitoring net cell pressure, pore water pressure, pore air pressure, and temperature while measuring changes in net cell pressure, pore water volume, soil total volume, and temperature during testing. A schematic and photo of the thermal isotropic cell control system are shown in Figures 1 and 2, respectively. The cylindrical vessel is made of 316 stainless steel with an outside diameter of 165.1 mm, a wall thickness of 9.5 mm, and a height of 157.2 mm. The cell is designed to accommodate specimens having a height of 25.4 mm and a diameter up to 71.12 mm. The stainless steel vessel can accommodate net cell pressures to 10 MPa. The top and base of the isotropic cell are also made of 316 stainless steel with a thickness of 29 mm and a diameter of 228.6 mm.

Mechanical Loading System

The mechanical loading system consists of a high pressure (CELL) flow pump developed as part of this study to apply and maintain the confining stress (i.e. cell pressure) of the soil specimen during testing. The CELL flow pump is capable of supplying pressures to the thermal

isotropic cell up to 10 MPa. Pressure is transferred from the flow pump to the isotropic cell through a 3.2 mm-diameter flexible 316 stainless steel line connected to the stainless steel base of the isotropic cell. The CELL flow pump operates by moving a cylindrical piston with a cross-sectional area of 4793 mm^2 within a reservoir made of 316 stainless steel filled with de-aired mineral oil (Crystal Plus 70T). The piston has an operating stroke length of 340 mm, yielding a total available cell fluid volume exchange of 1629.6 mL. A large operational volume is necessary during heating due to the relatively large coefficient of thermal expansion of the mineral oil (0.00063 1/°C). Movement of the piston during testing is controlled and monitored by a Stepnet controller (Model STX-115-07) manufactured by Copley Control Corp., with an operational velocity range of 0.00001 to 0.4 mm/s, corresponding to an apparent strain rate of 0.043 and 17265 %/hr, respectively for a 27 mm-tall, 67.1 mm-diameter specimen. However, the true strain rate of the soil specimen will be less than the apparent value due to the additional compression of the cell confining fluid.

Internal cell pressures are monitored within the isotropic cell using a 1400 kPa capacity pressure sensor, manufactured by Geotac©, installed at the base of the isotropic cell. For testing, the CELL flow pump controller is programmed to operate until a cell pressure equal to the target cell pressure ± 0.1 kPa has been achieved. This value was chosen as it is slightly larger than the observed noise of the cell pressure transducer. The flow pump remains inactive until the cell pressure exceeds the target cell pressure by ± 1.75 kPa. An activation pressure of 1.75 kPa was selected as it was found to reduce potential overshooting or excessive operation of the CELL flow pump during testing.

Pore Pressure Control System

The top and bottom soil caps are designed to allow for the independent distribution of water and air pressure to the soil specimen, respectively, following the axis-translation technique (Hilf 1956). The degree of saturation of the soil specimen is controlled/monitored using a "pore water pressure" (PWP) flow pump operating within a suction feedback-control loop which utilizes a differential pressure transducer (DPT) placed between the pore air and pore water pressure supply lines. A detailed schematic of the thermal isotropic cell, showcasing the pore pressure control system, is presented in Figure 3. The PWP flow pump is designed to be smaller than the CELL flow pump with a cylindrical piston active cross-sectional area of 791.73 mm^2 and an operating stroke length of 240 mm, yielding a total available pore water volume exchange of 190.01 mL. Movement of the piston is controlled and monitored by a Stepnet controller (Copley Control Corp) with a velocity range of 0.00001 to 4.0 mm/s, corresponding to flow rates of 7.9×10^{-3} to 3.2×10^{3} mm^3/s and an apparent Darcy velocity of 2.2×10^{-9} to 8.9×10^{-4} mm/s, respectively, for a soil specimen 67.1 mm in diameter. The Stepnet controller has the capability of measuring the location of the piston to 1×10^{-6} mm, giving the PWP flow pump the ability to measure changes in pore water volume as precise as 7.917×10^{-4} mm^3.

Operation of the PWP flow pump causes water to flow into or out of the soil specimen through a 7 mm-thick, 71.1 mm-diameter 1-bar high air entry value (HAEV) ceramic disk placed between the bottom soil cap and the soil specimen. This disk allows for the continuous and uniform application of water pressure to the bottom of the specimen without allowing the entry of air until reaching a suction of 100 kPa. Pore air pressure is distributed to the top of the specimen using a 6.45 mm-thick, 71.1 mm-diameter coarse porous stone placed between the soil and top cap to ensure a uniform application of air or water pressure throughout the top of the

specimen. The porous stone was experimentally determined to have a porosity of 0.368 corresponding to a saturated water volume of 9.42 mL. This information is used to correctly determine the amount of water expelled from the soil specimen during drying. To partition the soil specimen from the cell fluid, the soil specimen and top and bottom caps are sealed with a 0.635 mm-thick neoprene membrane. Neoprene was selected for testing as it provides a higher resistance to elevated temperatures than conventional rubber or latex membranes.

During the application of matric suction, the difference between the water pressure at the bottom of the specimen and the air pressure applied to the top of the specimen (during the application of matric suction) is measured using a Validyne (Model P305D) differential pressure transducer "DPT" (Fig. 3) containing a 3-38 diaphragm with an operating capacity of 55 kPa. Accordingly, the differential pressure transducer is used to monitor the matric suction at the bottom boundary of the specimen. The DPT output is monitored by a suction feedback-control loop developed by McCartney and Znidarčić (2010) to achieve different equilibrium values of matric suction within the soil specimen. As suction imposed by flow pump operation is only representative of the suction at the boundary of the specimen, the feedback loop is necessary to control the flow of water to or from the specimen for wetting and drying, respectively, until the matric suction at the boundary equilibrates with the suction in the rest of the specimen. For testing, the PWP flow pump controller is designed to stop operation of the piston once the target matric suction has been reached within ± 0.01 kPa, which is slightly larger than the observed noise of the pressure transducer. The PWP flow pump will remain inactive until the suction has reached a value equal to the target suction value ± 1.41 kPa. The soil is assumed to have achieved uniform suction throughout when the PWP flow pump has been non-operational for a

time of 5000 s. Additional details on the program operation used to dry or wet the soil specimen can be found in Lee and Znidarčić (2013).

Initial pore air and water pressures, prior to use of the PWP flow pump, are applied to the specimen through two independent burettes that are included in a pressure control panel manufactured by Trautwein Soil Testing Equipment Company. Each burette allows for the unique application of air/water pressure, vacuum pressure, or venting. This permits an easy transition from saturated to unsaturated control conditions as water within the burette controlling the top of the soil specimen may be flushed to transition from the application of pore water pressure to pore air pressure that is equal in magnitude. In addition, each burette is controlled and monitored by an independent pressure regulator and calibrated pressure gauge, respectively, to permit the precise application of pore water or pore air pressure to the soil specimen.

Temperature Control System

Changes in temperature are applied to the soil specimen by varying the temperature of the cell fluid located within the isotropic cell. The temperature of the cell fluid and soil specimen is regulated by circulating a heat exchange fluid through a 6.3 mm-diameter copper heating coil installed within the cell chamber. Water is used as the heat exchange fluid. The temperature of the heat exchange fluid is controlled using a F25-ME refrigerated/heating circulator from Julabo Inc., which consists of an automated temperature control system, fluid reservoir, and circulating pump, shown in Figure 3 and 4. The heat pump (Fig. 4b) has a working temperature range of -28 to 200 °C with a temperature control resolution of ± 0.1 °C and is capable of both heating and cooling. The circulating pump can supply a fluid pressure up to 38 kPa and a flow rate up to 16×10^3 mL/min.

The temperature control system also permits the precise ramping of temperature within the cell, allowing for the application of slow temperature rates of less than 0.3 °C/hr. Sultan et al. (2002) observed this rate to be acceptable to ensure full drainage of saturated specimens during heating. Temperature of the cell fluid is monitored and recorded using two Omega K-Type thermocouple probes mounted at the top and bottom of the isotropic cell (Fig. 3). In addition, the two thermocouples are utilized to monitor any thermal gradients that may develop during heating. The top and bottom thermocouple probes were designed to measure the temperature near the porous stone and HAEV stone, respectively, so all observed gradients may be assumed to occur along the height of the soil specimen. To minimize the temperature gradient, a 60 mm diameter – 14 mm deep high speed Evercool CPU cooling fan mounted at the top of the isotropic cell is used to circulate the cell fluid within the cell chamber [Fig. 4(a)]. Circulating speed of the fan is controlled using a HP Dual DC Power Supply (Model 6253A) that limits the voltage input to the CPU fan. For a target cell fluid temperature of 70 °C, operation of the CPU fan was observed to reduce the temperature gradient from 6 °C to less than 1.5 °C. A preliminary investigation showed operation of the circulatory fan to have no effect on cell pressure or signal output of the instrumentation. To minimize heat loss during testing, the aluminum isotropic cylinder is wrapped with two layers of 6.35 mm-thick thermal insulation.

Volume Change Measurement System

The direct measurement technique was chosen to measure changes in soil volume for the new high pressure thermal isotropic cell. Three non-contact proximity sensors (3300 XL 8 mm), manufactured by GE Bently Nevada, were selected to monitor changes in soil height and diameter based on changes in distance between the probe tip and a conductive AISI 4140 steel target. For the temperature range applied in testing (15 to 80 °C), the proximity sensors were

experimentally determined to have an operating range of 2.3 mm with a precision of ± 0.0005 mm. To infer changes in the soil diameter, two proximity probes are mounted radially around the soil specimen at mid height with a 60° offset as shown in Figure 5. These probes are hereby referred to as radial "Probe A" and radial "Probe B". Though the radial deformation of the soil can be monitored with one probe, two probes were chosen for redundancy as well as to assess the uniformity of deformation of the soil specimen. To measure changes in soil height, one proximity sensor is mounted vertically above the soil top cap (Figs. 3 and 5), hereby referred to as axial "Probe C". The volumetric strain of the soil under various loading conditions is calculated using the averaged radial displacements recorded from Probes A and B and the vertical deformation recorded from Probe C. The steel targets are 19 mm in diameter and 2.5 mm thick. The targets used for radial deformation measurement are rounded to a 34.5 mm radius on one side so that full contact may be achieved along the soil/neoprene surface. The targets are adhered to the neoprene membrane and soil top cap using Gorilla® super glue as it was found to not lose its adhesive properties when exposed to the mineral oil cell fluid for long periods of time. One concern that may arise is the increase in stress concentration to the soil specimen at the location of the radial probe targets. This would mostly be recognized by the appearance of increased deformations of the soil underneath the targets. However, no such deformations were observed for any tests so the possibility of stress concentrations along the soil may be disregarded. All three proximity probes are mounted to two Invar alloy brackets installed at the bottom of the cell chamber. Probe A is mounted to one bracket while Probes B and C share a second bracket (Fig. 5). Invar alloy was chosen as the mounting bracket material because of its low coefficient of thermal expansion (1.2×10^{-6} 1/°C), thereby reducing the relative movement between the probe and the steel target due to changes in temperature. Finally, a tech grade

mineral oil (Crystal Plus 70T) is used as the cell fluid due to its non-conductive properties which will prevent cross-talk between the probes.

Laboratory Environment

As changes in ambient room temperature can negatively impact the accuracy of experimental instrumentation, precision of the temperature controller system when operating at slow heating rates, and pressure maintained within the cell and PWP flow pumps during operation, a temperature-controlled laboratory located at the University of Colorado at Boulder was selected to house the thermal isotropic system for testing. A K-Type fine-wire thermocouple is installed near the thermal isotropic cell in order to monitor ambient room temperatures throughout testing. The room is maintained at a temperature of 19 °C (± 1.0 °C). A cooler temperature than the rest of the building is necessary to minimize the effects of entering or exiting the lab during testing.

CALIBRATION OF THERMAL ISOTROPIC CELL

Overview

Changes in cell pressure and/or temperature may cause deformations to the experimental equipment that will lead to changes in distance between the probe tip and steel target unrelated to the volume change of the soil. For radial Probes A and B, changes in cell pressure and/or temperature will cause a deformation of the soil specimen, neoprene membrane, steel target, and INVAR mounting bracket. For axial Probe C, changes in cell pressure and/or temperature will result in deformation of the soil specimen, top and bottom stainless steel soil caps, HAEV ceramic disk, coarse stone, and INVAR mounting bracket. In addition, changes in pressure or temperature along the probe may cause a small shift in sensor output voltage (GE Bentley Nevada 2013).

In order to accurately determine the volume change of the soil specimen it is necessary to characterize the thermo-mechanical "machine" deformations of the isotropic cell equipment. Knowledge of the thermo-mechanical response of the relevant components may then be used to correct the raw displacement data to infer the true soil deformation. As such, two independent testing procedures, both utilizing a 25.4 mm-tall, 63.5 mm-diameter aluminum "dummy" specimen with an elastic modulus of 68.9 GPa and a volumetric coefficient of thermal expansion of 69×10^{-6} 1/°C, were developed to determine the response of the isotropic equipment to changes in cell pressure and temperature. In general, the thermo-mechanical equipment deformations may be determined by applying an increase in either cell pressure or temperature to the aluminum specimen, then subsequently subtracting the expected deformation of the aluminum specimen from that measured by the displacement probes. The resulting deformation may then be used to determine the true thermo-mechanical deformation of a soil specimen in the axial (ΔH) or radial (ΔR) direction as defined in EQ. 2(a) and EQ. 2(b), respectively.

$$\Delta H\left(\Delta\sigma,\Delta T\right)=\Delta H_{measured}-\Delta H_{cal}\left(\Delta\sigma,\Delta T\right) \quad \text{EQ. 2(a)}$$

$$\Delta R\left(\Delta\sigma,\Delta T\right)=\Delta R_{measured}-\Delta R_{cal}\left(\Delta\sigma,\Delta T\right) \quad \text{EQ. 2(b)}$$

Mechanical Machine Deflections of Isotropic System

The mechanical machine deformation of the thermal isotropic system was evaluated in a mechanical calibration program so that they may be considered when interpreting changes in volume of the soil specimen due to changes in cell pressure. An aluminum specimen was subjected to a net confining stress of 350 kPa and a backpressure of 320 kPa then left overnight to achieve stabilization of the probes, mounting brackets, and steel targets prior to isotropic compression. Following this, the aluminum specimen was loaded from 350 to 1000 kPa at an average rate of 78 kPa/hr. Following achievement of the target cell pressure, the stress conditions

were held constant for several hours to assess any mechanical voltage drift of the probes which may occur (i.e. change in probe voltage output with no change in cell pressure). However, no voltage drift was observed indicating all mechanical system deformations had occurred during loading. The resulting mechanical machine deflections for all three probes are shown in Figure 6(a), where a positive deformation signifies a settlement of the equipment (i.e., an increase in the gap between probe tip and target) while a negative deformation indicates expansion of the equipment (i.e., a decrease in gap between probe tip and target). Radial probes A and B exhibit a very small decrease in gap during loading, while axial Probe C exhibits a larger increase in gap. This behavior is expected as Probe C will also measure the mechanical compression of the soil top and bottom caps, coarse stone, and HAEV disk which is expected to be larger than the compression of the neoprene membrane and stainless steel target alone. The mechanical deformation relationships of all three probes are defined by EQ. 3 through EQ. 5 below:

$$\Delta R_{cal,A}(\Delta\sigma) = -3.33\times10^{-9}(\sigma-\sigma_{BP})^2 - 5.9\times10^{-6}(\sigma-\sigma_{BP}) \quad \text{EQ. 3}$$

$$\Delta R_{cal,B}(\Delta\sigma) = -4.40\times10^{-10}(\sigma-\sigma_{BP})^2 - 3.8\times10^{-6}(\sigma-\sigma_{BP}) \quad \text{EQ. 4}$$

$$\Delta H_{cal,C}(\Delta\sigma) = 6.9\times10^{-4}\sqrt{\sigma-\sigma_{BP}} \quad \text{EQ. 5}$$

where σ is the current mean confining stress and σ_{BP} is the mean confining stress applied during backpressure saturation (350 kPa for the tests presented in this study).

Thermal Machine Deflections of Isotropic System

Following loading to 1000 kPa, the cell was heated from ambient temperature (≈ 21.5 °C) to a temperature of 67 °C to determine the thermal deformation of the isotropic system. The cell was heated in three distinct increments at a rate of 0.34 °C/hr, from ambient to 35 °C, 35 to 49 °C, and 49 to 67 °C. At the end of each increment, the temperature was held constant for

several hours to assess any additional thermal voltage drift of the probes which may occur (i.e. change in probe voltage output with no change in temperature). Similar to the mechanical deformation test, no voltage drift was observed indicating all thermal system deformations had occurred during heating. The resulting thermal machine deflections are shown in Figure 6(b). Similar to the results for the mechanical deformation test, axial Probe C shows more deformation than radial Probes A and B due to the presence of the suction control components. The thermal deformation relationships of all three probes are defined by EQ. 6 through EQ. 8 below:

$$\Delta R_{cal,A}(\Delta T) = -7.4\times10^{-6}(T-T_{amb})^2 - 1.2\times10^{-4}(T-T_{amb}) \quad \text{EQ. 6}$$

$$\Delta R_{cal,B}(\Delta T) = -1.1\times10^{-5}(T-T_{amb})^2 - 5.1\times10^{-5}(T-T_{amb}) \quad \text{EQ. 7}$$

$$\Delta H_{cal,C}(\Delta T) = -1.4\times10^{-5}(T-T_{amb})^2 - 1.2\times10^{-3}(T-T_{amb}) \quad \text{EQ. 8}$$

where T is the current average cell temperature and T_{amb} is the ambient average cell temperature prior to heating.

Calibration for Determination of Changes in Pore Water Volume

During the heating of soil, thermal expansion of water located within the pore drainage lines may occur resulting in withdrawal of the PWP flow pump that is unrelated to changes in the soil pore water volume. It is important to characterize the thermal expansion of water located within the drainage lines to properly calibrate for changes in the soil gravimetric water content due to changes in temperature. To do so, the pore water volume of the bottom drainage line (corresponding to the PWP flow pump) was monitored using a high accuracy pipette while heating an aluminum specimen from 21.5 to 67 °C. Negligible changes in bottom pore volume were observed.

In addition to the impact of changes in temperature on the pore plumbing network, variations in the ambient laboratory temperature may cause expansion or contraction of the de-aired water stored within the PWP flow pump reservoir which could result in operation of the PWP pump piston not associated with changes in volume of the pore water located within the soil specimen. To assess this potential behavior, the PWP flow pump was set to apply and maintain a target pore water pressure of 320 kPa to the bottom of the aluminum dummy specimen for 48 hours. During this 48 hours, the ambient laboratory temperature was allowed to fluctuate and the response of the PWP flow pump was monitored. The results are shown in Figure 7. For a variation in ambient lab temperature between 18.1 to 19.4 °C, no significant response of the PWP flow pump was observed. Therefore, the variations in ambient laboratory temperature are assumed to have negligible influence on the measurements made by the PWP flow pump for this study.

Some cases of cell fluid migration through neoprene membranes at elevated temperature have been observed in the literature (Cekerevac et al. 2005). To examine this behavior, the aluminum "dummy" specimen was loaded to a confining stress of 1000 kPa with a constant backpressure of 320 kPa, and then heated to 67 °C. Migration of the mineral oil cell fluid through the neoprene membrane was measured by monitoring two high accuracy pipettes individually attached to the top and bottom pore pressure supply lines. Over the time of 24 hours, no raise in water level for either pore pressure line was observed, indicating negligible migration of the cell fluid through the neoprene membrane at elevated temperatures. This lack of fluid migration may be due to the increased viscosity of the mineral oil compared to that of de-aired water.

Based on the observances described above, all movements of the PWP flow pump during testing may be assumed to only be due to changes in volume of the soil pore water. For all

drained heating or cooling tests, the thermal expansion/contraction of the soil solids and soil pore water has been considered for the calculation of changes in void ratio resulting degree of saturation. Specifically, the change in pore volume (ΔV_v) and change in volume of soil pore water (ΔV_w), has been modified to account for thermal expansion of the soil constituents. Throughout testing, changes in volume of the soil specimen are deduced based on linear deformations in the radial and axial directions measured using three non-contact displacement probes. During heating or cooling, the measured change in volume ($\Delta V_{t,measured}$) is assumed to be a summation of the change in volume of the voids and the thermal expansion (or contraction) of the soil solids:

$$\Delta V_{t,measured} = \Delta V_v + V_{s0}\alpha_{T,s}\Delta T \quad \text{EQ. 9}$$

where V_{s0} is the initial volume of the soil solids, and $\alpha_{T,s}$ is the thermal coefficient of volumetric expansion of the soil solids. For this study, $\alpha_{T,s}$ is assumed to be 3.5 × 10^{-5} 1/°C, as specified by Campanella and Mitchell (1968). The resulting change in pore volume during a change in temperature may be written as:

$$\Delta V_v\left(\Delta T\right) = \Delta V_{t,measured} - V_{s0}\alpha_{T,s}\Delta T \quad \text{EQ. 10}$$

Likewise, the change in volume of the soil pore water during heating or cooling must also be considered. Campanella and Mitchell (1968) proposed the following relationship considering the properties of free pure water:

$$\Delta V_w\left(\Delta T\right) = \Delta V_{w,measured} - V_{w0}\alpha_{T,w}\Delta T \quad \text{EQ. 11}$$

where $\Delta V_{w,measured}$ is the change in water volume measured by the PWP flow pump, and $\alpha_{T,w}$ is the thermal coefficient of volumetric expansion of the pore water, assumed to be equal to 2.07 × 10^{-4} 1/°C. Baldi et al. (1988) proposed a modification to EQ. 11 to incorporate the effects of

adsorbed water using the double layer theory for low porosity plastic clays. However, Delage et al. (2000) found the assumption of free water by Campanella and Mitchell (1968) to be sufficient for the evaluation of the thermal volume change of the pure water for Boom clay. Furthermore, the presence of pure water should be insignificant for the soil utilized in this study.

EXPERIMENTAL INVESTIGATION

Soil Preparation Procedures

A silt obtained from the Bonny dam located near the Colorado/Kansas border in Yuma County, CO was used to demonstrate the capabilities of the new thermo-hydro-mechanical true isotropic device. A summary of the relevant geotechnical properties for the silt are summarized in Table 1. The liquid and plastic limits of the soil are 25 and 21, respectively, measured in accordance with ASTM D4318, and the fines content is 83.9%. Accordingly, the silt is classified as ML (inorganic low plasticity silt) according to the Unified Soil Classification System (USCS, ASTM D2487). An activity of 0.29 indicates the silt does not contain a significant amount of active clay minerals.

The soil specimens in this study were prepared to a dry density of approximately 1450 kg/m^3 (void ratio of approximately 0.83) at a compaction gravimetric water content of 13.9% using static compaction. Specifically, a mechanical press was then used to compress the specimen in one 27 mm tall lift within a cylindrical aluminum mold 67.1 mm in diameter. Following compaction, the specimen was extracted from the aluminum mold. The compacted silt specimen was then weighed, and the dimensions were measured to determine the obtained initial conditions. The compaction conditions evaluated in this study are different than those on previous studies that evaluated the behavior of compacted Bonny silt: Khosravi and McCartney (2011) used a void ratio of 0.53 and a compaction water content of 14%, Coccia and McCartney

(2012) used a void ratio of approximately 0.46 and a compaction water content of 17.4%, and Alsherif and McCartney (2013, 2015) used a void ratio of 0.68 and a compaction gravimetric water content of 10.5%. The different compaction conditions are expected to lead to different hydraulic, mechanical, and thermal properties. The compression indices for the Cam-Clay model (λ and κ) the parameters of the soil-water retention curve (SWRC) model of van Genuchten (1980) (α_{vG}, n_{vG}, and $S_{r,res}$), the hydraulic conductivity (k), and the thermal conductivity (k_t) that are specific to the compaction conditions in this study are also summarized in Table 1.

Experimental Procedures

Following compaction, the soil specimen was set into the thermal isotropic cell atop the bottom cap and 1-bar ceramic disk and a neoprene membrane was placed around the sample. Next, the top and bottom pore pressure control plumbing was installed to the respective valve and fittings. A vacuum of 81.5 kPa was applied to the top of the soil specimen to seat the neoprene membrane to the soil circumference as well as to de-air the specimen to assist in saturation. Once the membrane was seated, a thin layer of super glue was applied to two radial steel targets which were then attached to the neoprene membrane at the corresponding locations for radial Probes A and B. Once the targets were sealed to the neoprene membrane, the Invar alloy probe brackets were mounted to the cell base and the corresponding displacement probes were installed. During setup, the probes were placed so that their tips would be approximately 0.75 mm away from the corresponding steel target. The probes were monitored for several minutes to ensure a constant signal output was achieved, indicating the glue had finally set and no target drift was occurring. Once confirmed, the remaining components of the thermal isotropic cell were assembled and the cell chamber was filled with de-aired mineral oil and a small seating pressure of 50 kPa was applied. The top vacuum was reduced to 68 kPa and de-

aired water was flushed upwards from the bottom of the specimen by imposing a bottom pore water pressure of 20 kPa. De-aired water was allowed to flush through the top of the soil specimen until a volume of water equivalent to two pore volumes had passed through the soil and air bubbles were no longer observed coming from the top of the soil specimen, which on average took 5-6 hours. The vacuum at the top of the specimen was turned off and switched to a pore water pressure of 20 kPa, equal to that applied at the bottom of the soil specimen. The total stress (50 kPa) and backpressure (20 kPa) were increased in stages of 35 kPa until a total stress of 350 kPa and a backpressure of 320 kPa was achieved. The compacted specimen was not observed to exhibit any significant change in volume during this process. The soil was left to backpressure saturate overnight. This technique was observed to achieve an average B-value of around 0.96, and was considered sufficient for saturation. Once the specimen was saturated, the CPU circulatory fan was turned on and left for the rest of testing.

Following backpressure saturation, the remainder of the experimental testing of the compacted silt was carried out via three distinct stages: (1) Application of matric suction; (2) Mechanical isotropic consolidation to a target total stress; (3) Drained heating. The initial soil conditions for the three tests performed to showcase the capabilities of the high pressure thermal isotropic cell are summarized in Table 2. The thermo-mechanical response of a saturated normally consolidated soil specimen is tested in Test S-0. Test US-30A was performed to investigate the hydro-thermo-mechanical response of an unsaturated normally consolidated soil specimen. Test US-30B was performed to confirm the achieved suction-saturation relationship determined in Test US-30A. The hydro-thermo-mechanical stress paths performed for the three tests are summarized in Figure 8. The standard procedures for testing following saturation is described as follows:

1. Application of matric suction of 30 kPa for Tests 2 and 3 using the PWP flow pump. Pore water was removed from the soil specimen by withdrawing the piston of the PWP flow pump at a rate of 0.0001 mm/s which corresponds to an apparent Darcy velocity of 2.23×10^{-8} m/s (500 times slower than the saturated hydraulic conductivity of the silt).
2. Mechanical isotropic consolidation of the specimens for Tests S-0 and US-30A to a total mean stress of 1000 kPa. Specimens were loaded in constant rate of strain conditions with a constant CELL flow pump piston velocity of 4×10^{-5} and 2×10^{-5} mm/s. This corresponds to apparent strain rates of 0.173 and 0.086 %/hr for Tests S-0 and US-30A, respectively. This includes both soil and machine deformations. A slow loading rate was chosen to avoid the generation of excess pore water pressure during loading so that the compression curve of the soil may be fully characterized.
3. Drained heating of Tests S-0 and US-30A to a target temperature of ≈ 65 °C at a rate of 0.35 °C/hr. Heating was performed in three stages from ambient temperature to 35 °C, 35 to 48 °C, and 48 °C to 63 °C, and the temperature was held until equilibrium was reached at each stage.

Experimental Results

Results from the desaturation tests (Test US-30A and US-30B) at ambient room temperature are shown in Figure 9. For both tests, a target suction of 30 kPa was applied to the soil specimen via withdrawal of the piston from the reservoir of the PWP flow pump. A total stress of 350 kPa was held constant during desaturation. The suction response with time as well as the corresponding change in pore water volume is shown in Figure 9(a) and 9(b), respectively. Initially, the measured matric suction is relatively low until a sudden increase is occurs around 25 and 20 hours for Tests US-30A and US-30B, respectively [Figure 9(a)]. This jump in matric

suction value corresponds to completion of drainage of the coarse stone placed atop the soil specimen. The volume of pore water withdrawn at this time must be properly calibrated to calculate the final degree of saturation for the soil specimen once equilibrium conditions are met. A small contraction of the soil specimen also occurred following final desaturation of the coarse stone as seen in Figure 9(c). A continuous increase in matric suction is observed until the target suction value of 30 kPa is achieved. At which point, the measured suction corresponds to the value at the bottom boundary of the soil specimen. The PWP flow pump continues an ON/OFF operation procedure to maintain the suction value within the pre-defined threshold value (30 kPa ± 1.41 kPa). Once this threshold has been met for longer than 5000 s, the suction and water content distribution along the soil height is assumed to be uniform. For both tests, this process took about 125 hours. For a matric suction of 30 kPa, degrees of saturation of 0.569 and 0.554 were attained for Tests US-30A and US-30B, respectively [in Fig. 9(d)]. The degree of saturation was calculated based on the amount of water withdrawn (calibrated following drainage of the coarse stone) along with any changes in soil volume that occurred. Agreement between Tests US-30A and US-30B indicates reliable operation of the saturation/suction control system.

Results from the isotropic mechanical drained consolidation tests for saturated (Test S-0) and unsaturated (Test US-30A) specimens of compacted silt are shown in Figure 10. During loading, a backpressure value of 320 kPa was maintained for Test S-0, while the PWP flow pump was utilized to maintain a constant suction value of 30 kPa for the unsaturated specimen in Test US-30A. Maximum loading rates of 4.98 and 10.15 kPa/hr were measured to correspond with the CELL flow pump piston velocities of 2×10^{-5} and 4×10^{-5} mm/s, respectively (Fig. 10a). To assess the ability of the non-contact displacement probes to measure changes in soil volume, as well as to investigate the uniformity of soil deformation during loading, the volumetric strain calculated

using displacement measurements from Axial Probe C and either Radial Probe A or B for Tests S-0 and US-30A are shown in Figure 10(b). For Test S-0, final volumetric strains of 6.9% and 7.2% were calculated based on the displacements recorded by Radial Probe A and Radial Probe B, respectively, along with Axial Probe C. For Test US-30A, no significant discrepancy is observed based on volume change calculations using either radial probe. Unless a significant issue is observed for either radial probe throughout testing, final volume change calculations are calculated using an average displacement of the two radial probes. The change in degree of saturation with mean effective stress for Test US-30A is shown in Figure 10(c). A very small decrease in degree of saturation of 0.0024 is observed during initial loading to a mean effective stress of around 170 kPa, followed by an increase in degree of saturation of about 0.0208. The overall increase in degree of saturation with increasing total stress is expected due to the accompanied decrease in void ratio of the soil specimen that will cause a shift of the air entry suction value to larger values of matric suction (Gallipoli et al. 2003). The compression curves for Tests S-0 and US-30A are shown in Figure 10(d). For this study, the mean effective stress of the soil specimen σ′ was calculated using the definition of generalized of effective stress as described by Bishop and Blight (1963):

$$\sigma' = (\sigma - u_a) + S_r(u_a - u_w) \qquad \text{EQ. 9}$$

where σ is the mean total stress, u_a is the pore air pressure, u_w is the pore water pressure, and S_r is the degree of saturation. For the saturated specimen in Test S-0, exchanges in pore water volume during mechanical loading or unloading may be used to determine the change in volume of the bulk soil, assuming the soil solids to be incompressible (Uchaipichat and Khalili 2011). As such, for Test S-0, fluctuations in the volume of soil pore water were monitored during the mechanical loading stage using a high-accuracy burette to compare with the volume change

results in Figure 10(d), calculated using the non-contact displacement probes. Excellent agreement between the burette readings and non-contact displacement probe measurements was observed for the evolution of void ratio with mean effective stress (Fig. 10d), confirming the capability of the adopted soil volume measurement technique to reliably measure mechanically induced volumetric strains. In the effective stress space, the slope of the isotropic normal compression line, λ, was determined to be 0.069, and appears to be independent of matric suction [Fig. 10(d)]. Further, an increase in mean effective preconsolidation stress was observed with increasing matric suction from 0 to 30 kPa. This impact of matric suction on the slopes of the compression curve and mean effective preconsolidation stress was also observed by Uchaipichat and Khalili (2009) for specimens of compacted silt. A small amount of secondary creep was also measured following achievement of the target total stress, resulting in an additional decrease in void ratio of around 0.005 for both Tests S-0 and US-30A. The mechanical strain anisotropy for both tests was also assessed during mechanical loading. The axial and radial strains with mean effective stress for Tests S-0 and US-30A is shown in Figure 10(e). Larger deformations were observed in the axial direction than in the radial direction for both tests. The relationship between axial and radial strain during drained mechanical loading may be defined by the anisotropic mechanical strain ratio ($\varepsilon_{aT} / \varepsilon_{rT}$) that is the ratio of axial to radial strain. The anisotropic mechanical strain ratio versus mean effective stress is shown in Figure 10(f). During initial loading, the anisotropic mechanical strain ratio is slightly scattered and increases from 0 to approximately 1.25 for both tests. The abrupt variance in the strain ratio is expected to be due to the initially low magnitude of mechanical axial and radial strains where small changes in radial or axial strain will result in a large change in the strain ratio. After initial loading, the anisotropic mechanical strain ratio is observed to stabilize and steadily increase to an

average anisotropic mechanical strain ratio of 1.82 and 1.98 for Tests S-0 and US-30A, respectively.

Results from the drained heating tests on the saturated (Test S-0) and unsaturated (Test US-30A) specimens of compacted silt are shown in Figure 11. Heating was initiated for each test once the observed volumetric strain rate from the previous isotropic mechanical loading stage was less than 0.0005 %/hr. This procedure was followed in order to isolate the thermal volumetric strain of the soil specimen during heating from excess secondary creep following the previous loading increment. During heating, a mean total stress of 1000 kPa was maintained using the CELL flow pump for both tests. In addition, a backpressure value of 320 kPa was maintained for Test S-0, while a constant suction value of 30 kPa was maintained for the unsaturated specimen in Test US-30A, using the PWP flow pump. A maximum heating rate of 0.34 °C/hour was measured for both tests as shown in Figure 11(a). The thermal volumetric strain with time for Tests S-0 and US-30A is shown in Figure 11(b), where positive volumetric strain indicates contraction. The rate of thermal volumetric strain is observed to decrease dramatically when the soil temperature is held constant. This indicates the heating rate of approximately 0.3 °C/hour to be small enough to avoid the development of thermally induced excess pore water pressure. For Test S-0, final thermal volumetric strains of 0.488% and 0.565% were calculated using Radial Probe A and Radial Probe B, respectively. For Test US-30A, final thermal volumetric strains of 0.583% and 0.678% were calculated using Radial Probe A and Radial Probe B, respectively. In general, the volumetric strain trends and relative magnitudes are in agreement. The change in degree of saturation with temperature for US-30A is shown in Figure 11(c). The degree of saturation was observed to decrease by 0.0024. During heating, a change in saturation will occur due to the cumulative effects of a decreasing void ratio (for the

case of normally consolidated soils) and increasing temperature. The results in Figure 10(d) indicate that a decreasing void ratio will cause an increase in the degree of saturation due to an increase in the air entry value. However, increases in temperature will cause a decrease in the air entry suction due to the decrease in viscosity of the pore water resulting in a reduction in interfacial tension between the pore water and soil solids (Romero et al. 2001). The observed decrease in degree of saturation for Test US-30A during heating suggests the impact of temperature on the air entry suction to dominate the adjoined effect of the decrease in void ratio. This behavior was also observed by Uchaipichat and Khalili (2009).

The thermal volumetric strain with temperature is shown in Figure 11(d) for Tests S-0 and US-30A. Both soil specimens exhibited contraction with increases in temperature as expected for a soil heated in normally consolidated conditions (Cekerevac and Laloui 2004). The saturated specimen was observed to exhibit a smaller averaged rate of thermal volumetric strain ($\varepsilon_{vT} / \Delta T$), 0.0085 %/°C, than for the unsaturated specimen, 0.0103 %/°C. The thermal strain anisotropy for both tests was also assessed during heating. The axial and radial strains with mean effective stress for Tests S-0 and US-30A is shown in Figure 11(e). Similar to that during mechanical loading, larger deformations were observed in the axial direction than in the radial direction for both tests. These results differ from those observed by Hueckel and Pellegrini (1996) who found larger strains to occur in the radial direction during heating. The relationship between axial and radial strain during drained mechanical loading may be defined by the anisotropic thermal strain ratio ($\varepsilon_{aT} / \varepsilon_{rT}$) that is the ratio of axial to radial strain. The anisotropic mechanical strain ratio versus mean effective stress is shown in Figure 11(f). During initial heating, the anisotropic thermal strain ratio is highly variable due to the low magnitude of thermal radial strains relative to the measured thermal axial strains. At a temperature of around 35 °C, the anisotropic thermal

strain ratio is observed to stabilize and exhibit a steady decrease with increasing temperature with a much more exaggerated decrease observed for Test S-0. After heating, an average thermal strain ratio of 4.30 and 3.48 was measured for Tests S-0 and US-30A, respectively.

The thermal strain rates measured for Tests S-0 and US-30A are in agreement with other data from the literature, summarized in Figure 12(a). The thermal strain rate determined for Tests S-0 and US-30A for a change in temperature of 30 °C is compared with the thermal strain results from Uchaipichat and Khalili (2009) in Figure 12(b) on normally consolidated compacted Bourke silt of various initial degrees of saturation. For the Bonny silt, the thermal strain rate was observed to increase with decreasing degree of saturation, while the opposite was measured for the Bourke silt as determined by Uchaipichat and Khalili (2009). However, more tests are required to assess the complete relationship between the initial degree of saturation and thermal volumetric strain for NC soils.

Finally, to validate the capability of the PWP flow pump to accurately measure changes in the volume of the pore water under various stress paths based on the assumptions of the thermal expansion of free water by Campanella and Mitchell (1968), the gravimetric water content as determined by operation of the PWP flow pump was compared with the experimentally measured water content of the unsaturated soil specimen of Test US-30A following extraction. The evolution of gravimetric water content with time for the suction application stage, mechanical loading stage, and drained heating stage determined by the PWP flow pump is shown in Figure 13 and is compared with the final measured gravimetric content. Good agreement is observed between the extracted gravimetric water content with that measured by the PWP flow pump. As such, the assumption of the thermal expansion of free water, as proposed by

Campanella and Mitchell (1968), is sufficient to determine the true variation in the volume of pore water during heating.

CONCLUSIONS

This paper described the development of a new high pressure thermo-hydro-mechanical isotropic cell used for the evaluation of the thermal volume change mechanisms of saturated and unsaturated soils. The thermal isotropic cell is capable of applying and maintaining matric suction/degree of saturation, temperature, and isotropic net mean stresses (up to 10 MPa) at very slow rates to fully characterize the soil compression and volume change curves for soils at various initial degrees of saturation. Volume changes of the soil specimen throughout testing are monitored using three non-contact proximity transducers, avoiding the need to consider complex thermo-mechanical cell deformations. Further, variations in degree of saturation may be measured during changes in net stress, matric suction, and temperature. A preliminary study on three compacted silt specimens under two different initial degrees of saturation was executed to highlight the capabilities of the high pressure thermo-hydro-mechanical isotropic cell as well as to assess the impact of degree of saturation on mechanical and thermal volume change behavior. The test results indicate matric suction/degree of saturation to not impact the slope of the normal compression line in the effective stress space. However, an increase in suction was observed to increase the soil's mean effective preconsolidation stress. The degree of saturation of the unsaturated specimen was observed to increase with net stress due to the resulting decrease in void ratio. During heating, the degree of saturation was observed to decrease as a result of decreasing pore water viscosity with increasing temperature. The saturated soil specimen was observed to exhibit a smaller thermally induced volumetric strain than the unsaturated specimen. However, more testing is required to assess the impact of initial degree of saturation on the

thermal volumetric strain of normally consolidated soils. Further, the saturated and unsaturated soil specimens were observed to exhibit larger strains in the axial deformation than in the radial direction during changes in mean effective stress and temperature.

ACKNOWLEDGEMENTS

The authors appreciate the support from National Science Foundation grant CMMI-1054190. The views in this paper are those of the authors alone.

REFERENCES

Abuel-Naga, H.M., Bergado, D.T., Bouazza, A. and Ramana, G.V., 2007, "Volume Change Behaviour of Saturated Clays under Drained Heating Conditions: Experimental Results and Constitutive Modeling," *Canadian Geotechnical Journal*, Vol. 44, pp. 942-956.

Alsherif, N.A. and McCartney, J.S. (2015). "Nonisothermal behavior of compacted silt at low degrees of saturation." Géotechnique. 65(9), 703-716. DOI: 10.1680/geot./14-P-049.

Alsherif, N., and McCartney, J.S., 2013, "Triaxial Cell for Nonisothermal Shear Strength of Compacted Silt under High Suction Magnitudes," *Proceedings of the 1st Pan-American Conference on Unsaturated Soils*, Cartagena de Indias, pp. 147-152.

Baldi, G., Hueckel, T., and Pelegrini, R., 1988, "Thermal Volume Changes of the Mineral-Water System in Low-Porosity Clay Soils," *Canadian Geotechnical Journal*, Vol. 25, pp. 807-825.

Bellia, Z., Ghembaza, M.S., and Belal, T., 2015, "A Thermo-Hydro-Mechanical Model of Unsaturated Soils Based on Bounding Surface Plasticity," *Computers and Geotechnics*, Vol. 69, pp. 58-69.

Bishop, A.W., and Blight, G.E., 1963, "Some Aspects of Effective Stress in Saturated and Unsaturated Soils," *Géotechnique*, Vol. 13, No. 3, pp. 177–197.

Bishop, A.W., and Donald, I.B., 1961, "The Experimental Study of Partly Saturated Soil in Isotropic Apparatus," *5th International Conference on Soil Mechanics and Foundation Engineering*, Paris, pp. 13-21.

Burghignoli A., Desideri A., and Miliziano S., 2000, "A Laboratory Study on the Thermomechanical Behaviour of Clayey Soils," *Canadian Geotechnical Journal*, Vol. 37, pp. 764-780.

Campanella, R.G., and Mitchell, J.K., 1968, "Influence of Temperature Variations on Soil Behavior," *Journal of the Soil Mechanics and Foundation Engineering Division*, Vol. 94, No. SM3, pp. 9-22.

Cekerevac, C., and Laloui, L., 2004, "Experimental Study of Thermal Effects on the Mechanical Behavior of a Clay," *International Journal for Numerical Analytical Methods Geomechanics*, Vol. 28, pp. 209–228.

Cekerevac, C., Laloui, L., and Vulliet, L., 2005, "A Novel Triaxial Apparatus for Thermo-Mechanical Testing of Soils," *Geotechnical Testing Journal*, Vol. 28, No. 2, pp. 1-10.

Coccia, C.J.R., and McCartney, J.S., 2012, "A Thermo-Hydro-Mechanical True Triaxial Cell for Evaluation of the Impact of Anisotropy on Thermally-Induced Volume Changes in Soils," *ASTM Geotechnical Testing Journal*, Vol. 35, No. 2, pp. 227-237.

Coccia, C.J.R., and McCartney, J.S., 2013, "Impact of Heat Exchange on the Thermo-Hydro-Mechanical Response of Reinforced Embankments," *Proc. Geocongress 2013*, ASCE, pp. 343-352.

Cui, Y.J., Le, T.T., Tang, A.M., Delage, P., and Li, X.L., 2009, "Investigating the Time-Dependent Behaviour of Boom Clay Under Thermomechanical Loading," *Géotechnique*, Vol. 59, No. 4, pp. 319-329.

Cui, Y. J., Sultan, N., and Delage, P., 2000, "A Thermomechanical Model for Clays," *Canadian Geotechnical Journal*, Vol. 37, No. 3, pp. 607–620.

Delage, P., Sultan, N., and Cui, Y.J., 2000, "On the Thermal Consolidation of Boom Clay," *Canadian Geotechnical Journal*, Vol. 37, pp. 343-354.

Demars, K.R., and Charles, R.D, 1982, "Soil Volume Changes Induced by Temperature Cycling," *Canadian Geotechnical Journal*, Vol. 19, pp. 188–194.

François, B., and Laloui, L., 2008, "ACMEG-TS: A Constitutive Model for Unsaturated Soils under Non-Isothermal Conditions." *International Journal for Numerical and Analytical Methods in Geomechanics*, Vol. 32, pp. 1955-1988.

Gallipoli, D., Wheeler, S.J., and Karstunen, M., 2003, "Modelling the Variation of Degree of Saturation in a Deformable Unsaturated Soil," *Géotechnique*, Vol. 53, No. 1, pp. 105-112.

GE Bentley Nevada, 2013, "3300 XL 8 mm Proximity Transducer System," Specifications and Ordering Information, pp. 1-35.

Hilf, J.W., 1956, An Investigation of Pore-Water Pressure in Compacted Cohesive Soils, Ph.D. Thesis, University of Colorado, Department of Civil Engineering, Denver.

Hueckel, T., and Baldi, M., 1990, "Thermoplasticity of Saturated Clays: Experimental Constitutive Study," *Journal of Geotechnical Engineering*, Vol. 116, No. 12, pp. 1778–1796.

Hueckel, T., and Pellegrini, R., 1992, "Effective Stress and Water Pressure in Saturated Clays during Heating-Cooling Cycles," *Canadian Geotechnical Journal*, Vol. 29, pp. 1095-1102.

Hueckel, T., and Pellegrini, R., 1996, "A Note on Thermomechanical Anisotropy of Clays," *Engineering Geology*, Vol. 41, pp. 171-180.

Khosravi, A., and McCartney, J.S., 2011, "Resonant column test for unsaturated soils with suction–saturation control." *ASTM Geotechnical Testing Journal*, Vol. 34, No. 6, pp. 730-739.

Lee, J., and Znidarčić, D., 2013, "Flow Pump System for Unsaturated Soils: Measurement of Suction Response and the Soil–Water Retention Curve," *Geotechnical Testing Journal,* Vol. 36, No. 5, pp. 1-12.

Macari, E.J., Parker, L.K., and Costes, N.C., 1997, "Measurement of Volume Changes in Triaxial Tests Using Digital Imaging Techniques," *Geotechnical Testing Journal*, Vol. 20, No. 1, pp. 103–109.

McCartney, J.S., and Znidarčić, D., 2010, "Testing System for Hydraulic Properties of Unsaturated Nonwoven Geotextiles," *Geosynthetics International*, Vol. 17, No. 5, pp. 355-363.

Murphy, K.D., McCartney, J.S., and Henry, K.H., 2015, "Thermo-Mechanical Response Tests on Energy Foundations with Different Heat Exchanger Configurations," *Acta Geotechnica*. Vol. 10, No. 2, pp. 179-195.

Paaswell, R.E., 1967, "Temperature Effects on Clay Soil Consolidation," *Journal of the Soil Mechanics and Foundation Engineering Division*, Vol. 93, No. SM3, pp. 9–22.

Plum, R. L., and Esrig, M. I., 1969, "Some Temperature Effects on Soil Compressibility and Pore Water Pressure," *Effects of Temperature and Heat on Engineering Behavior of Soils*, Highway Research Board, No. 103, pp. 231–242.

Romero, E., 1999, *Characterization and Thermo-Hydro-Mechanical Behavior of Unsaturated Boom Clay: An Experimental Study*, Ph.D Thesis, Technical University of Catalonia, Department of Geotechnical Engineering and Geosciences, Spain.

Romero, E., Gens, A., and Lloret, A., 2001, "Temperature Effects on the Hydraulic Behaviour of an Unsaturated Clay," *Geotechnical and Geological Engineering*, Vol. 19, pp. 311-332.

Romero, E., Villar, M.V., and Lloret, A., 2005, "Thermo-Hydro-Mechanical Behaviour of Two Heavily Overconsolidated Clays," *Engineering Geology*, Vol. 81, pp. 255-268.

Saix, C., Devillers, P., and El Youssoufi, M.S., 2000, "Éléments de Couplage Thermomécanique Dans la Consolidation de Sols Non Saturés," *Canadian Geotechnical Journal*, Vol. 37, pp. 308- 317.

Salager, S., François, B., El Youssoufi, M.S., Laloui, L., and Saix, C., 2008, "Experimental Investigations of Temperature and Suction Effects on Compressibility and Pre-Consolidation Pressure of a Sandy Silt," *Soils and Foundations*, Vol. 48, No. 4, pp. 453-466.

Stewart, M., Coccia, C.J.R., McCartney, J.S, 2014, "Issues in the Implementation of Sustainable Heat Exchange Technologies in Reinforced Unsaturated Soils," *Proc. GeoCongress 2014,* ASCE, pp. 4066-4075.

Sultan, N., Delage, P. and Cui, Y.J., 2002, "Temperature Effects on the Volume Change Behavior of Boom Clay," Engineering Geology, Vol. 64, pp. 135-145.

Tang, A.M., 2005, *Effect de La Temperature sur le Comportement des Barrieres de Confinement*, Ph.D. Dissertation, Ecole Nationale des Ponts et Chaussees, Paris.

Tang, A.M., Cui, Y.J., and Barnel, N., 2008, "Thermo-Mechanical Behaviour of a Compacted Swelling Clay," *Géotechnique*, Vol. 58, No. 1, pp. 45-54.

Tavallali, A., Tang, A.M., and Cui, Y.J., 2007, "Thermo-Hydro-Mechanical Behaviour of Compacted Bentonite," *Experimental Unsaturated Soil Mechanics*, Vol 112, pp. 259-265.

Tidfors, M., and Sällfors, G., 1989, "Temperature Effect on Preconsolidation Pressure," *Geotechnical Testing Journal,* Vol. 12, No. 1, pp. 93–97.

Towhata, I., Kuntiwattanakul, P., Seko, I., and Ohishi, K., 1993, "Volume Change of Clays Induced by Heating as Observed in Consolidation Tests," *Soils and Foundations*, Vol. 33, No. 4, pp. 170–183.

Uchaipichat, A., and Khalili, N., 2009, "Experimental Investigation of Thermo-Hydro-Mechanical Behavior of an Unsaturated Silt," *Géotechnique*, Vol. 59, No. 4, pp. 339–353.

Uchaipichat, A., Khalili, N., and Zargarbashi, S., 2011, "A Temperature Controlled Isotropic Apparatus for Testing Unsaturated Soils," *Geotechnical Testing Journal*, Vol. 34, No. 5, pp. 1-9.

Vega, A. and McCartney, J.S., 2014, "Cyclic Heating Effects on Thermal Volume Change of Silt." Environmental Geotechnics, pp. 1-12. http://dx.doi.org/10.1680/envgeo.13.00022.

Wheeler, S.J., Sharma, R.J., and Buisson, M.S.R., 2003, "Coupling of Hydraulic Hysteresis and Stress-Strain Behaviour in Unsaturated Soils," *Gèotechnique*, Vol. 53, No. 1, pp. 41-54.

Zhou, A-N., Sheng, D., Sloan, S.W., and Gens, A., 2012, "Interpretation of Unsaturated Soil Behaviour in the Stress – Saturation Space, I: Volume Change and Water Retention Behaviour," *Computers and Geotechnics*, Vol. 43, pp. 178-187.

LIST OF TABLE CAPTIONS

TABLE 1: Summary of geotechnical properties of Bonny silt
TABLE 2: Summary of soil and testing conditions

LIST OF FIGURE CAPTIONS

FIG. 1: Schematic of the thermo-hydro-mechanical isotropic control system
FIG. 2: Photo of the high pressure thermal isotropic cell control system
FIG. 3: Detailed schematic of isotropic cell
FIG. 4: Temperature control system: (a) Photo of circulatory fan and top thermocouple; (b) Photo of thermal system
FIG. 5: Photo of assembly for radial (Probes A and B) and axial (Probe C) deformation measurement
FIG. 6: Cell deformations: (a) Mechanical; (b) Thermal
FIG. 7: PWP flow pump piston operation during room temperature swing
FIG. 8: Hydro-thermo-mechanical stress paths
FIG. 9: Desaturation test results for Tests US-30A and US-30B: (a) Suction results with time; (b) Change in soil pore water with time; (c) Change in soil volume with time; (d) Transient suction-saturation and equilibrium point
FIG. 10: Isotropic consolidation test results for Tests S-0 and US-30A: (a) Mean total stress with time; (b) Volumetric strain with time using Radial Probes A and B; (c) Degree of saturation with mean effective stress for Test US-30A; (d) Compression curves for Tests S-0 and US-30A; (e) Axial and averaged radial strains with mean effective stress; (f) Anisotropic strain ratio with mean effective stress
FIG. 11: Drained heating test results for Tests S-0 and US-30A: (a) Temperature with time; (b) Volumetric strain with time using Radial Probes A and B; (c) Degree of saturation with temperature for Test US-30A; (d) Thermal volume change curves; (e) Axial and averaged radial strains with temperature; (f) Anisotropic strain ratio with temperature
FIG. 12: (a) Thermal volumetric strain rate versus plasticity index for various soils; (b) Comparison between thermal volumetric strain values for silty soils under different degrees of saturation
FIG. 13: Gravimetric water content during testing for Test US-30A in comparison with measured value following specimen extraction

TABLE 1: Summary of geotechnical properties of Bonny silt

Parameter	Value
D_{10}	< 0.0013 mm
D_{30}	0.022 mm
D_{50}	0.039 mm
% Fines smaller than 75 μm	83.9%
% Sand size	16.1%
Liquid Limit, LL	25
Plastic Limit, PL	21
Plasticity Index, PI	4
Activity, A	29
Hydraulic conductivity, k	1.2×10^{-5} m/s
Isotropic compression index, λ	0.069
Isotropic recompression index, κ	0.006
van Genuchten SWRC parameter, α_{vG}	0.2 kPa^{-1}
van Genuchten SWRC parameter, n_{vG}	1.3
Residual saturation, $S_{r,res}$	0.05
Thermal conductivity, k_t	1.3 W/(m°C)

TABLE 2: Summary of soil and testing conditions

Test	Initial void ratio, e_0	Initial dry density, ρ_d	Compaction gravimetric water content, w_0	ψ(B)	ψ(C)	OCR	Temperature Sequence (D)
	(-)	(kg/m^3)	(%)	(kPa)	(kPa)	(-)	(°C)
S-0	0.83	1445	13.9	0	1000	1	21-35-48-62
US-30A	0.81	1460	13.9	30	1000	1	21-35-48-63
US-30B	0.75	1510	13.9	30	N/A	N/A	N/A

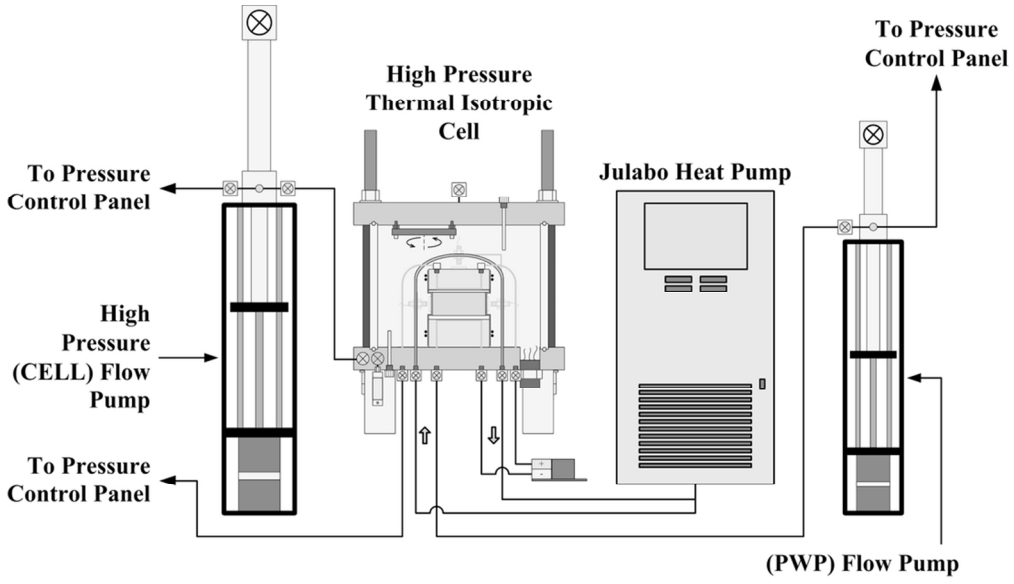

FIG. 1: Schematic of the thermo-hydro-mechanical isotropic control system
92x53mm (300 x 300 DPI)

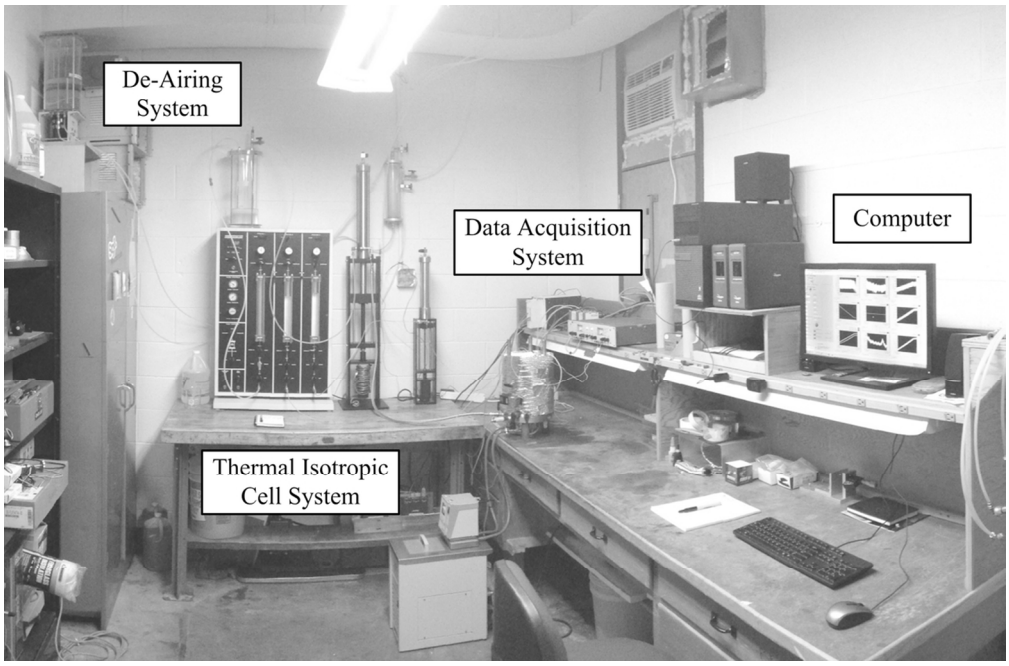

FIG. 2: Photo of the high pressure thermal isotropic cell control system
108x70mm (300 x 300 DPI)

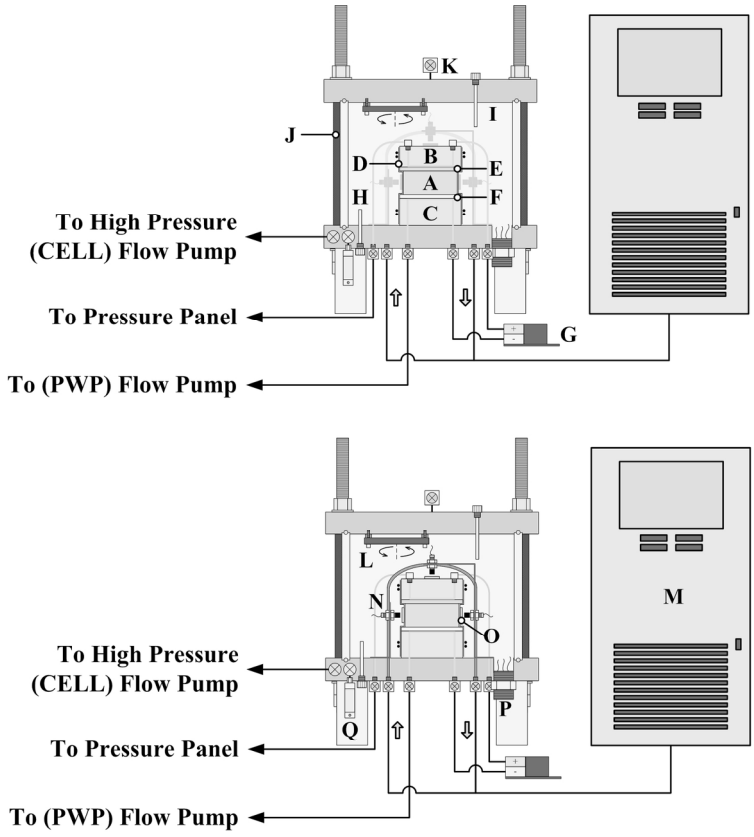

A: Soil Specimen; **B:** Top Soil Cap; **C:** Bottom Soil Cap; **D:** Neoprene Membrane; **E:** Coarse Porous Stone; **F:** High Air Entry Value Disk; **G:** DPT (for matric suction); **H:** Thermocouple Probe (bottom); **I:** Thermocouple Probe (top); **J:** Thermal Insulation; **K:** Cell Fluid Bleed Valve; **L:** Circulatory Fan; **M:** Julabo Heat Pump; **N:** Displacement Probes; **O:** Steel Target; **P:** HP Probe Feedthrough; **Q:** Cell Pressure Transducer

FIG. 3: Detailed schematic of isotropic cell
167x175mm (300 x 300 DPI)

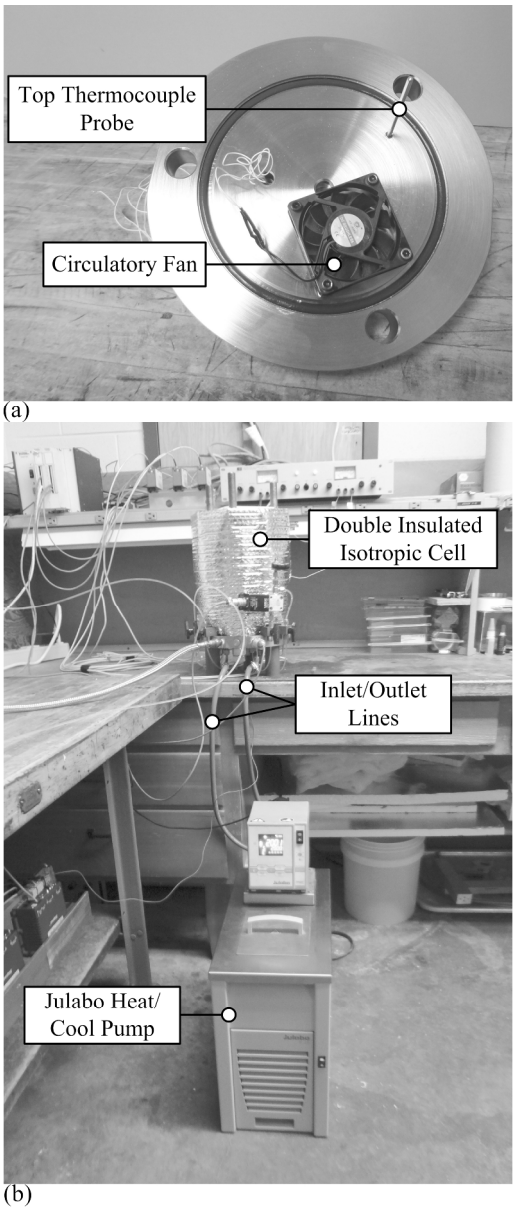

FIG. 4: Temperature control system: (a) Photo of circulatory fan and top thermocouple; (b) Photo of thermal system
209x493mm (300 x 300 DPI)

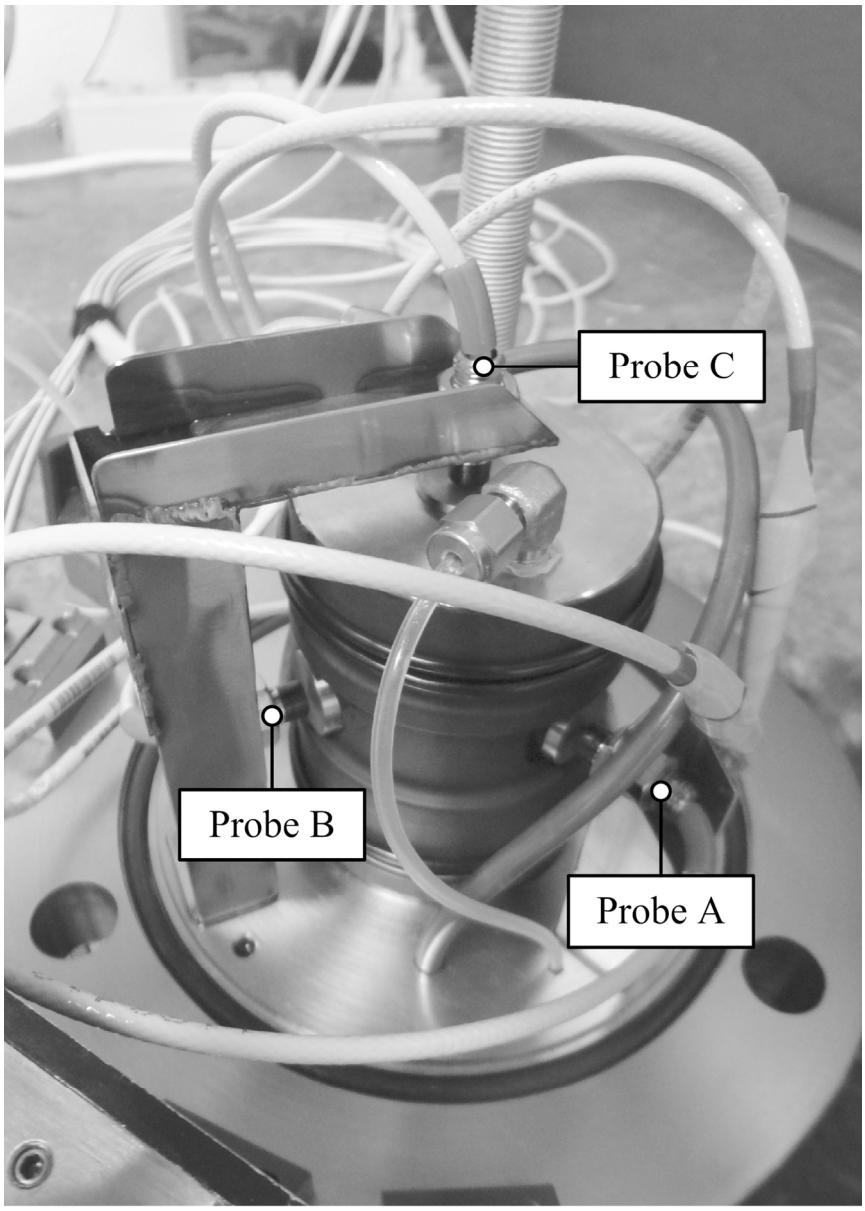

FIG. 5: Photo of assembly for radial (Probes A and B) and axial (Probe C) deformation measurement
124x174mm (300 x 300 DPI)

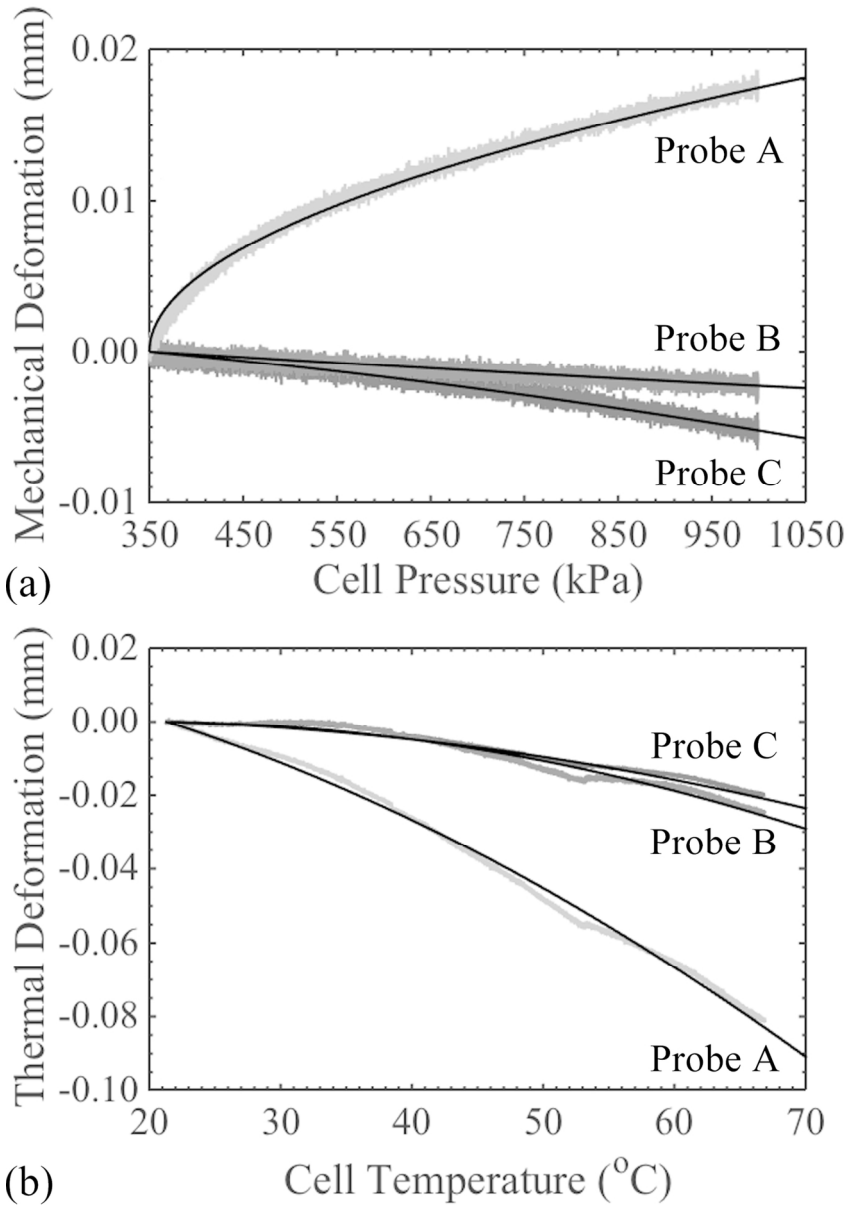

FIG. 6: Cell deformations: (a) Mechanical; (b) Thermal
120x164mm (300 x 300 DPI)

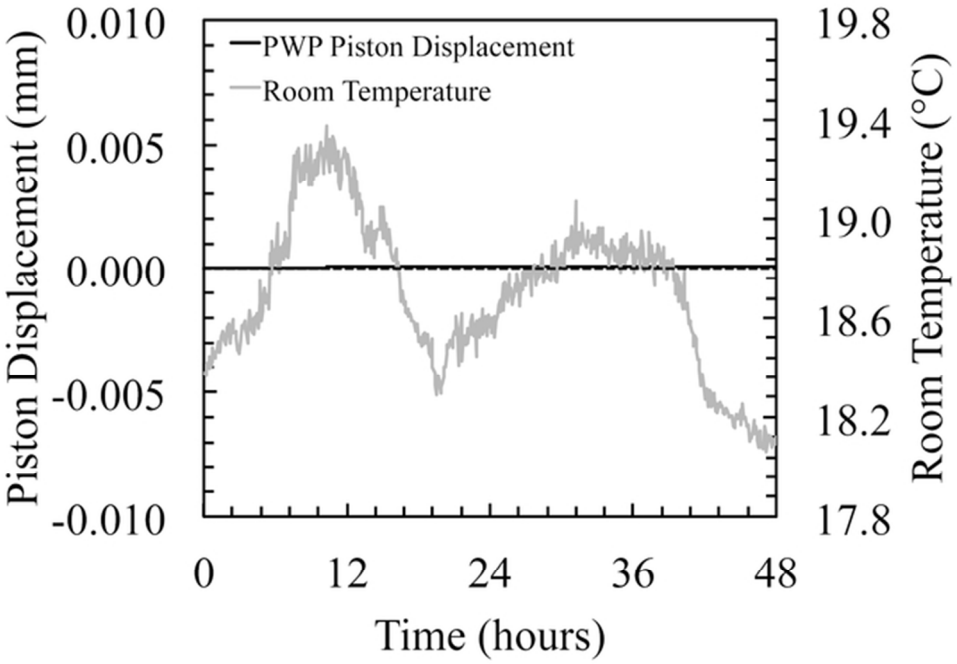

FIG. 7: PWP flow pump piston operation during room temperature swing
60x41mm (300 x 300 DPI)

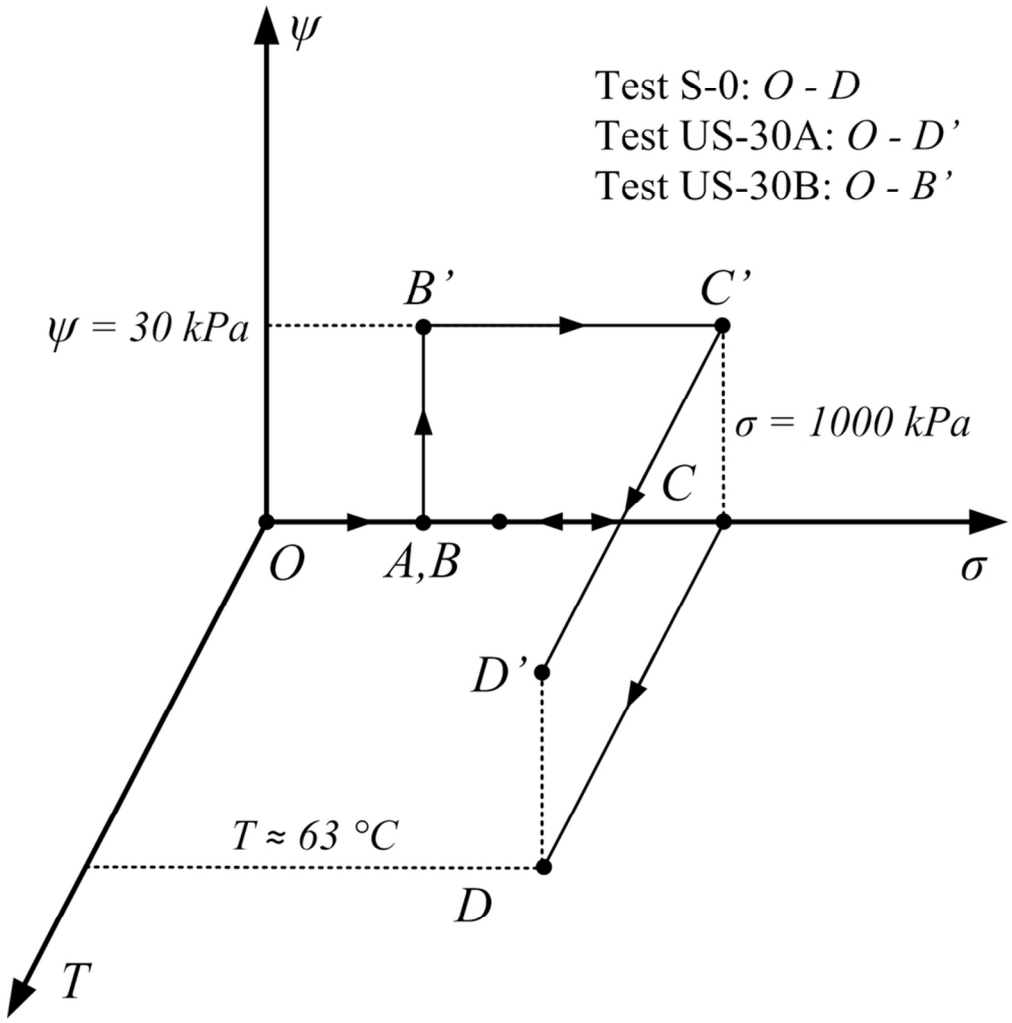

FIG. 8: Hydro-thermo-mechanical stress paths
84x87mm (300 x 300 DPI)

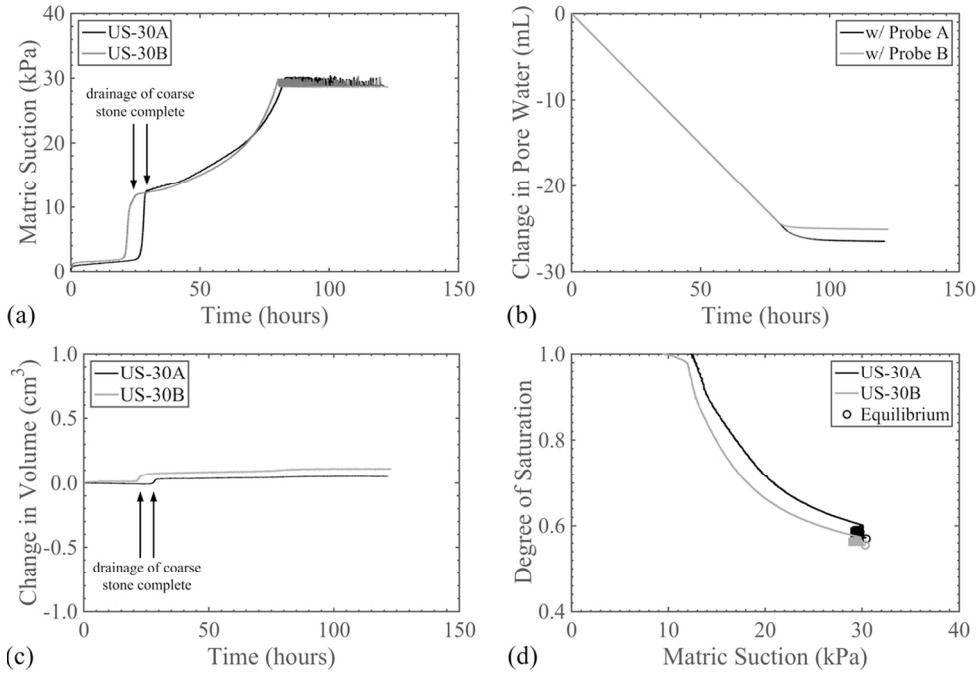

FIG. 9: Desaturation test results for Tests US-30A and US-30B: (a) Suction results with time; (b) Change in soil pore water with time; (c) Change in soil volume with time; (d) Transient suction-saturation and equilibrium point
112x76mm (300 x 300 DPI)

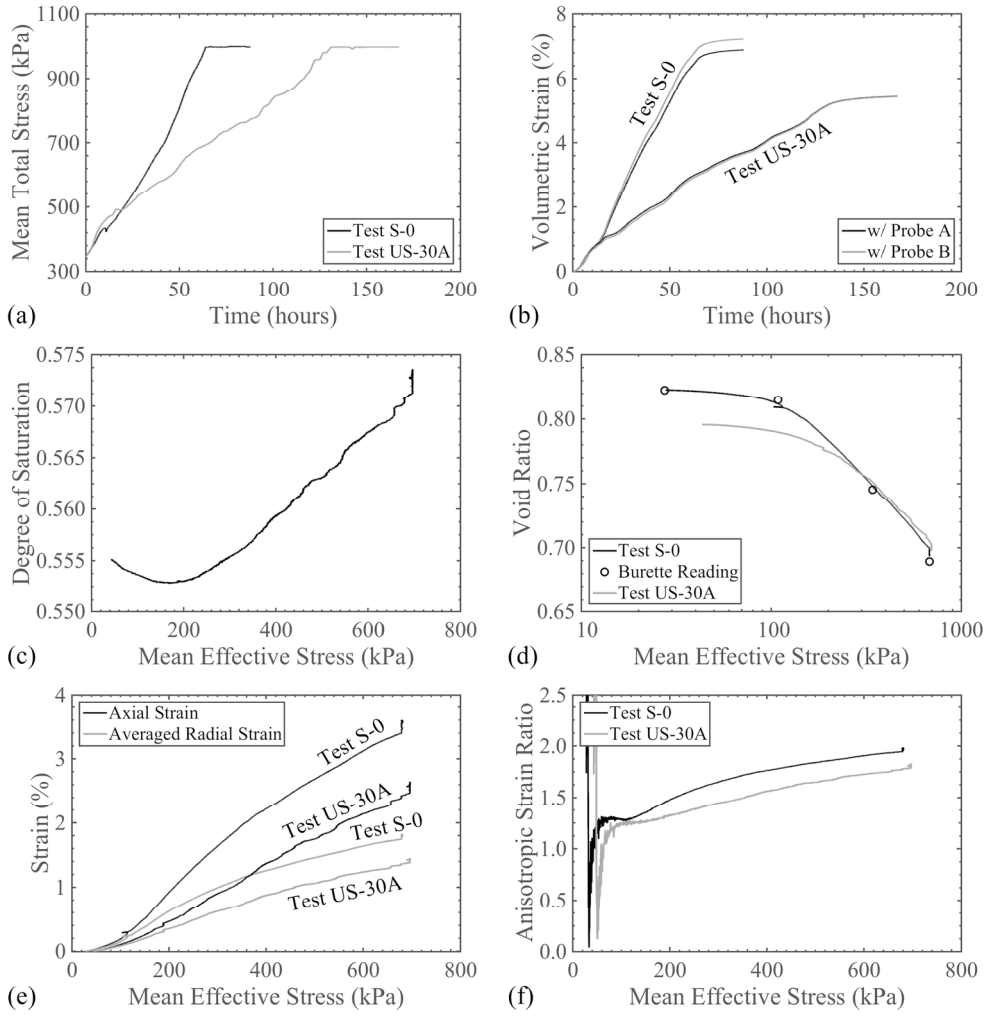

FIG. 10: Isotropic consolidation test results for Tests S-0 and US-30A: (a) Mean total stress with time; (b) Volumetric strain with time using Radial Probes A and B; (c) Degree of saturation with mean effective stress for Test US-30A; (d) Compression curves for Tests S-0 and US-30A; (e) Axial and averaged radial strains with mean effective stress; (f) Anisotropic strain ratio with mean effective stress
168x171mm (300 x 300 DPI)

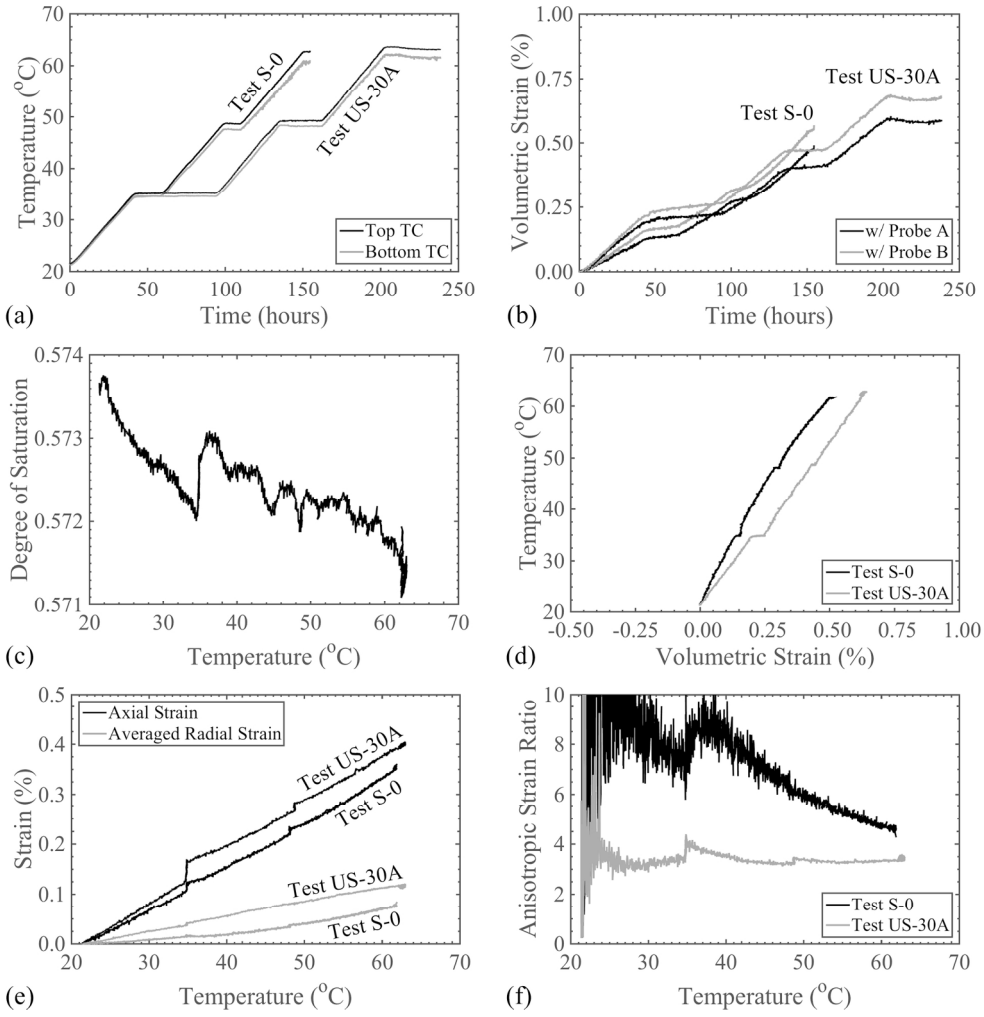

FIG. 11: Drained heating test results for Tests S-0 and US-30A: (a) Temperature with time; (b) Volumetric strain with time using Radial Probes A and B; (c) Degree of saturation with temperature for Test US-30A; (d) Thermal volume change curves; (e) Axial and averaged radial strains with temperature; (f) Anisotropic strain ratio with temperature
168x171mm (300 x 300 DPI)

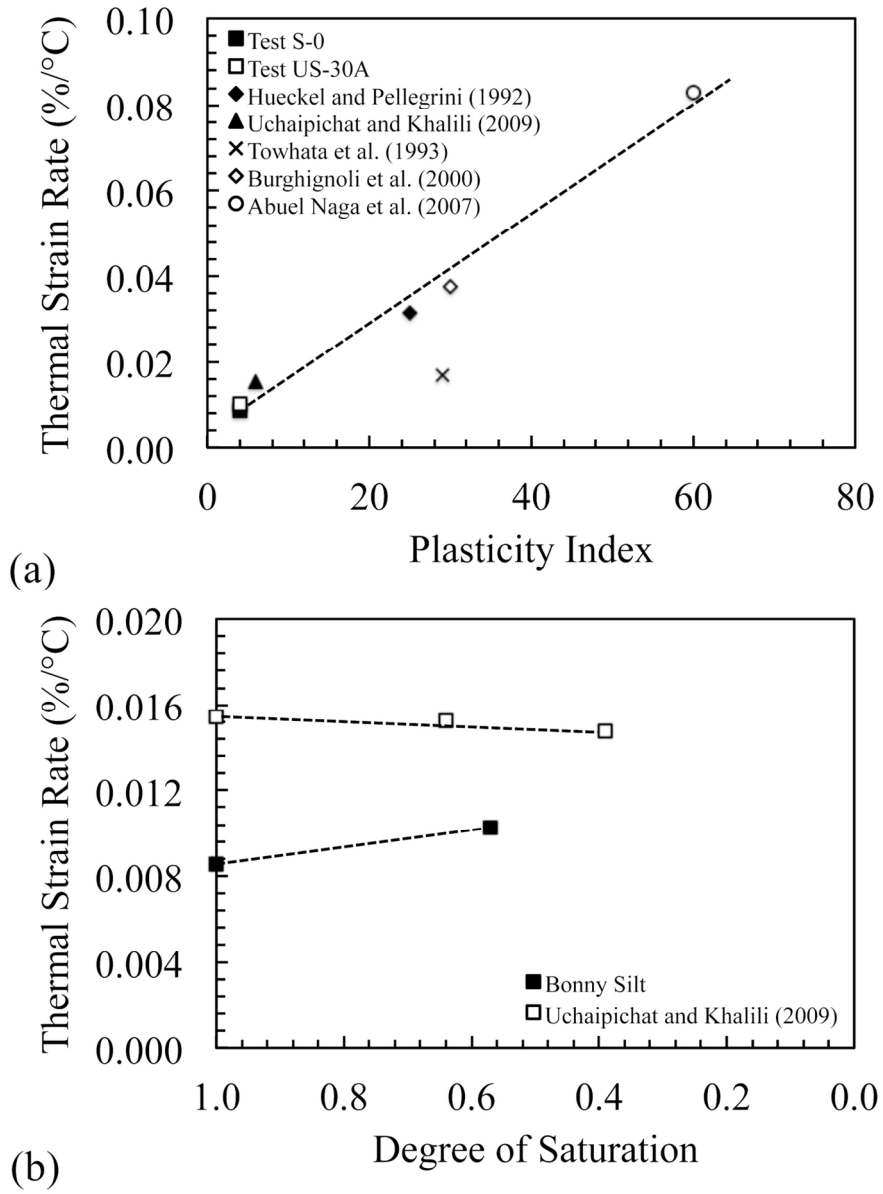

FIG. 12: (a) Thermal volumetric strain rate versus plasticity index for various soils; (b) Comparison between thermal volumetric strain values for silty soils under different degrees of saturation
120x163mm (300 x 300 DPI)

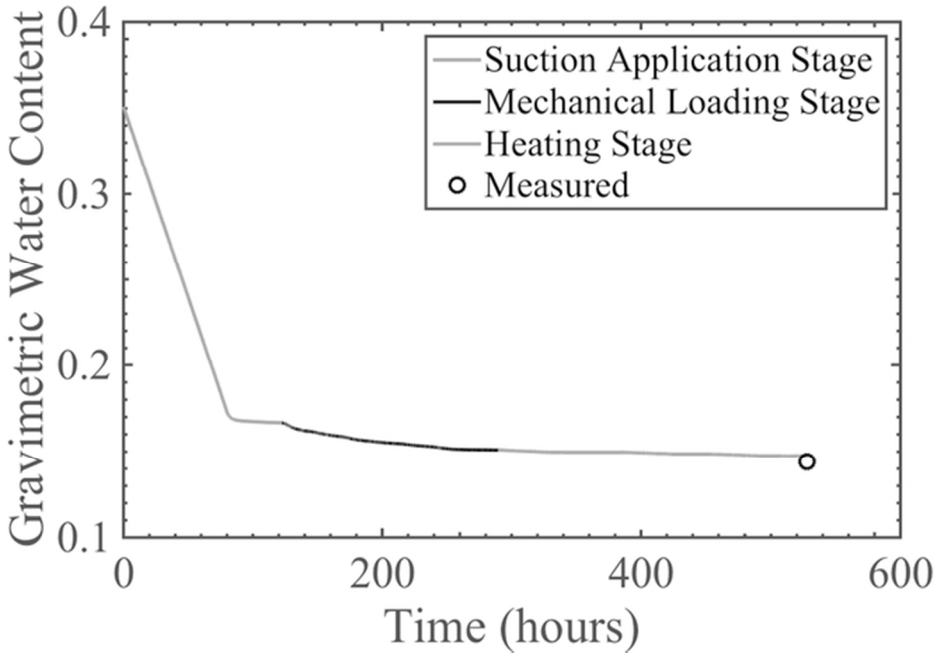

FIG. 13: Gravimetric water content during testing for Test US-30A in comparison with measured value following specimen extraction
60x41mm (300 x 300 DPI)